1-1-2018

Mechanical Property Development and Numerical Modeling of Ultra-High Performance Concrete Focused on Isothermal Curing Conditions

Thomas Allard

Mechanical property development and numerical modeling of ultra-high performance concrete focused on isothermal curing conditions

By

Thomas Allard

A thesis
Submitted to the Faculty of
Mississippi State University
in Partial Fulfillment of the Requirements
for the Degree of Master of Science
in Civil Engineering
in the Bagley College of Engineering

Mississippi State, Mississippi

December 2018

Mechanical property development and numerical modeling of ultra-high performance concrete focused on isothermal curing conditions

By

Thomas Allard

Approved:

_____

Isaac L. Howard
(Major Professor)

_____

Matthew W. Priddy
(Co-Major Professor)

_____

Jameson Shannon
(Committee Member)

_____

Farshid Vahedifard
(Graduate Coordinator)

_____

Jason M. Keith
Dean
Bagley College of Engineering

Name: Thomas Allard

Date of Degree: December 14, 2018

Institution: Mississippi State University

Major Field: Civil Engineering

Major Professor: Isaac L. Howard

Title of Study: Mechanical property development and numerical modeling of ultra-high performance concrete focused on isothermal curing conditions

Pages in Study 61

Candidate for Degree of Master of Science

Ultra-high performance concrete (UHPC) has progressively gained interest because of its favorable strength and durability properties. Literature shows that curing temperature has a significant effect on the resultant mechanical properties of UHPC, generally resulting in increased compressive strength. However, limited datasets are currently available to ascertain the degree of change related to compressive strength as a function of curing temperature and conditions. This study investigates the effect of isothermal and submerged curing temperature conditions, ranging from 10°C to 90°C, on the compressive strength and elastic modulus development of UHPC and generates a numerical model to capture these effects. The extent and rate of compressive strength development in Cor-Tuf UHPC was found to increase with curing temperature, while only the rate of elastic modulus development increased with curing temperature. The numerical model shows reasonable agreement when compared with the experimental results and was successfully implemented in finite element analysis software.

DEDICATION

Thanks are due to my parents for their continual love, support, and encouragement as I pursued my dream of higher education.

ACKNOWLEDGEMENTS

Thanks are due to the United States Army Corps of Engineers (USACE) Engineer Research Development Center (ERDC) for supporting this project (Chris Moore, Dr. Robert Moser, and several others have provided support in several manners). Thanks are due to my major professor and committee members: Dr. Isaac Howard, Dr. Matthew Priddy, and Dr. Jameson Shannon. Thanks are also due to Brad Hansen, Ashley Carey, Joseph Arthur, Michael Walsleben, Tanner Rhodes, Jim Steele, Brittni Cooper, Nicki Haines, and Garner Nance for items such as testing, data reduction, and overall project support.

This material is based upon work supported by the Military Engineering R&D program of ERDC supported by TARDEC under Contract No. W56HZV-17-C-0095 (PE 0602784A Project T53-Military Engineering Applied Research Task 08) and contract W56HZV-08-C-0236. Any opinions, findings, and conclusions or recommendations expressed in this material are those of the author and do not necessarily reflect the views of the U.S. Army TACOM Life Cycle Command. Dr. Clay Walden of the Center for Advanced Vehicular Systems (CAVS) was the leader of this work program, and Dr. Isaac Howard was the principal investigator for the tasks associated with this thesis.

DISTRIBUTION STATEMENT A. Approved for public release; distribution unlimited.

TABLE OF CONTENTS

LIST OF TABLES

LIST OF FIGURES

LIST OF SYMBOLS AND ACRONYMS

a_E	Scaling Rate Parameter for Elastic Modulus
a_f	Scaling Rate Parameter for Compressive Strength
ACI	American Concrete Institute
ASTM	American Society for Testing Materials
b_E	Exponent Rate Parameter for Elastic Modulus
b_f	Exponent Rate Parameter for Compressive Strength
c_0 to c_8	Fit coefficients for Compressive Strength
C_{469}	ACI 318 E to f_c proportionality constant
COV	Coefficient of Variation
d_0 to d_8	Fit coefficients for Elastic Modulus
E	Elastic Modulus
E_{23}	Elastic Modulus measurement adjusted to testing at 23°C
E_a	Activation Energy
E_{dial}	Elastic Modulus measured with analog dial method
E_{lim}	Hyperbolic Limiting Elastic Modulus term
E_{LVDT}	Elastic Modulus measured with LVDT method
ERDC	Engineer Research Development Center
f_c	Compressive Strength
f_{lim}	Hyperbolic Limiting Compressive Strength term
FHWA	Federal Highway Administration
GETVRM	Material Point Information Utility Subroutine
HRWRA	High Range Water Reducing Admixture
HSC	High Strength Concrete
i	Index term
I	Isothermal curing group
j	Index term
k	Hyperbolic rate term
k_E	Hyperbolic rate term for Elastic Modulus
k_f	Hyperbolic rate term for Compressive Strength
LVDT	Linearly Variable Displacement Transducer
M	Mixed temperature curing group
MAPE	Mean Absolute Percent Error
n	Number of specimens considered
n_j	Number of data points in curing group j
N	Total number of data points; sum of n_j over all j
R	Gas Constant; $8.314*10^{-3}$ kJ/K-mol
R^2	Coefficient of Determination
Q	Activation Energy divided by Gas Constant
RH	Relative Humidity
RMC	Ready Mixed Concrete
RMSPE	Root Mean Square Percent Error

SCM	Supplementary Cementitious Material
Δt	Time increment
t	Time
t_0	Time offset term
ΔT	Temperature increment
T	Temperature
T_0	Datum Temperature for C1074 maturity calculation
UHPC	Ultra-High Performance Concrete
USACE	United States Army Corps of Engineers
USDFLD	User Defined Field Variable Subroutine
V	Variability of Elastic Modulus with Temperature curing group
V_f	Fiber fraction by mixture volume
w/cm	Water-to-Cementitious Materials ratio
W_f	Fiber fraction by mixture weight
μ	Average
σ	Standard Deviation

CHAPTER I

INTRODUCTION

1.1 Introduction

Ultra-High Performance Concrete (UHPC) is a class of cementitious materials characterized by higher compressive strengths (f_c), reduced permeability, and increased toughness/durability relative to typical ready mixed concrete (RMC), partly due to steel fiber reinforcement. The gradation of constituent materials is selected to create a tightly packed system with a discontinuous pore structure that limits moisture ingress (e.g. condensed silica fume decreases and improves mechanical properties through pozzolanic reactions). Over the last 30 years, research by the United States Army Corps of Engineers (USACE) Engineer Research and Development Center (ERDC) to optimize material constituents has led to a version of UHPC, referred to as Cor-Tuf, which is the subject of this thesis (Williams et al. 2009; Green 2015).

The material constituents and their proportions in UHPC differ from conventional concrete systems in several ways, one of which is a higher cement content. As cement content increases, concrete mixtures have been shown to develop higher temperatures at early ages due to the chemical hydration reaction of cement and water (Gajda 2007). As shown through literature and in this experimental study, rate and extent of material property development for laboratory cylinders of UHPC tend to depend heavily on curing conditions

(e.g. temperature and moisture availability). Therefore, it can be expected that predicting mechanical property development within a UHPC structure requires knowledge of the temperature and moisture distributions and their effects.

The contents of this thesis represent a portion of ongoing research at Mississippi State University (MSU) with USACE ERDC that aims to better understand this material. Current laboratory and modeling efforts by MSU are aligned to accomplish two goals: 1) develop a numerical framework that can relate thermal and mechanical properties of laboratory experiments for various UHPC mixtures to full-scale field applications, and 2) implement predictive numerical models that can iteratively simulate construction conditions to better inform decision making relative to mix selection, structural design, and construction details/events (e.g. formwork type, timing of concrete placement, etc.).

This thesis shows through literature review and laboratory experiments that elevated temperature curing of UHPC often leads to higher f_c, but similar elastic modulus (E), as compared to ambient condition curing. The literature review was helpful to compare classes of UHPC, curing methods, and resulting mechanical property development trends; however, few studies were identified on the extent of temperature effects and rate of mechanical property development.

This dataset and numerical model provide a step toward understanding, predicting, and controlling the development of mechanical properties of UHPC in full-scale applications where mass concrete is of particular interest. Most of the content and results shown in this thesis are intended to be developed into to a paper submitted for peer-review with the main differences being additional literature review, more thorough investigation

of provisions outlined by American Society for Testing Materials (ASTM) standard practice C1074, and implementation of the numerical model in finite element software.

1.2 Objective

The first objective of this thesis is to investigate the rate and extent that constant temperature curing conditions effect the development of mechanical properties in laboratory cylinders of Cor-Tuf UHPC.

The second objective of this thesis is to develop a numerical model that captures the investigations of the first objective with a set of temperature-dependent functions that describe elastic modulus and compressive strength of Cor-Tuf UHPC and implement it in the Abaqus finite element analysis software.

1.3 Scope

This investigation is conducted through literature review, experimental testing, and numerical analysis. Literature review presents several studies that have shown UHPC and conventional concretes to respond differently to a variety of curing temperatures and conditions. The experimental studies presented consider a more thorough range of curing temperatures than seen in literature. Literature shows that few numerical models have been presented for the development of UHPC mechanical properties and are not suited to accurately capture curing effects using directly measured mechanical properties (f_c and E) as model inputs.

This thesis presents a systematic experimental program in which Cor-Tuf UHPC specimens are cured in three ways: 1) submerged in water bath in isothermal conditions, 2) standard moist curing room in isothermal conditions and 3) combination of mixed

temperature conditions in a moist curing room followed by water bath. The term "isothermal conditions" is used herein to generalize constant temperature curing once a cylinder is removed from its mold about 1 day after mixing the concrete. Although it is well known that the temperature of concrete varies with time in real applications, the isolated effects of temperature are evaluated independently by subjecting concrete cylinders to isothermal conditions at 6 curing temperatures (10, 23, 30, 50, 70, and 90°C). Specimens subjected to isothermal conditions are tested for mechanical properties over a continuous range of maturities (up to 2500°C-days), calculated according to ASTM C1074.

Test results of standard moist curing at 23°C is compared to water bath curing to investigate the importance of moisture availability for mechanical property development. Additional comparisons to isothermal curing are made with specimens cured at a combination of temperatures. These mixed temperature curing conditions are similar to standard conditions reported in literature; one of which has been used by ERDC and MSU extensively.

A numerical model is presented that modifies a hyperbolic function suggested by Carino et al. (1984) for conventional concrete. This model accounts for rate and extent of mechanical property development as a function of time and curing temperature for laboratory cylinders of Cor-Tuf UHPC cured in water baths under isothermal conditions. Parametric functions are fit to test data by minimizing the difference between measurements and predicted values using an optimization package in Python. The model is then discretized and implemented in a FORTRAN subroutine with the Abaqus finite element analysis software.

CHAPTER II

LITERATURE REVIEW

This literature review is divided into four sections corresponding to material background of UHPC (section 2.1), mechanical property development of UHPC for various curing conditions (section 2.2), prediction of concrete mechanical properties for laboratory experiments (section 2.3), and a brief discussion of full-scale modeling and prediction techniques for conventional concrete and UHPC structures (section 2.4). Literature is discussed by subject and focused toward the experimental and modeling goals of this thesis.

2.1 Materials Background

In the 1970s, considerable interest in high strength concrete (HSC) began with target strengths of 42 MPa (6 ksi) (Shah et al. 2017). Currently, American Concrete Institute (ACI) Committee 363 defines the lower limit for HSC to be 55 MPa (8 ksi), but makes the distinction that constituent material properties and production techniques are not drastically altered to achieve this limit (ACI 363). ERDC has made considerable mixture alterations, which differ from the ACI definition of HSC, for further strength improvement of cementitious systems. To achieve high strength and durability, research efforts have investigated use of oil-well cements, supplementary cementitious materials (SCMs) like silica fume, manufactured fine aggregates (e.g. silica sand and silica flour), low water-to-

cementitious materials ratio (w/cm), high range water reducing admixtures (HRWRA), and steel fiber reinforcement. Ultimately, this research led to the development of Cor-Tuf UHPC (Green 2015; Williams et al. 2009).

The Federal Highway Administration (FHWA) defines UHPC as cementitious composites with w/cm less than 0.25, discontinuous internal fiber reinforcement, f_c over 150 MPa (21.7 ksi), and post-cracking tensile strength over 5 MPa (0.72 ksi) (Graybeal 2006). High cement content (e.g., 900 to 1000 kg/m^3 or 1517 to 1686 lb/yd^3) replaces a large portion of aggregate volume and contributes to strength gain as compared with conventional concrete (e.g., 356 to 534 kg/m^3 or 600 to 900 lb/yd^3) (Gajda 2007; Liu et al. 2017). Due to the fine ingredients, steel fibers, and low w/cm, UHPCs typically require high-shear mixing. Field applications of UHPC have largely made use of proprietary premixes where a proportioned blend of ingredients were delivered to the customer (Graybeal 2011). Several research efforts characterizing the behavior of premix UHPCs have been performed previously (Ahmad and Hakeem 2015; Alsalman 2017; Graybeal 2011; Habel et al. 2006; Wan et al. 2016). The cost of UHPC premix materials can be 10 to 20 times that of conventional mixtures (Berry et al. 2017).

2.2 Mechanical Properties in Conjunction with Curing Temperature

There are potential benefits of high temperature curing producing favorable UHPC mechanical properties (e.g. mass concrete). Standard concrete curing is conducted in accordance with ASTM C192 in a moist curing room at 100% relative humidity (RH) and 21 to 25°C. Various methods have been employed to elevate curing temperature of laboratory specimens beyond 21 to 25°C including hot water baths, steam curing, and microwave curing. Table 2.1 summarizes several studies that characterize f_c and E of

UHPC under a variety of curing conditions and fiber fractions in which elevated temperatures resulted in higher f_c compared to the same mixture cured at ambient temperature (Ahmad and Hakeem 2015; Graybeal 2006; Howard et al. 2018a; Korpa and Trettin 2008; Prem et al. 2015; Sbia et al. 2017; Wan et al. 2016). For different UHPCs, elevated temperature curing increased f_c by 9 to 53% (Ahmad and Hakeem 2015; Graybeal 2006; Howard et al. 2018a; Prem et al. 2015; Wan et al. 2016), while E only increased by 8 to 16% (Ahmad and Hakeem 2015; Graybeal 2006; Howard et al. 2018a). Elastic modulus tends to increase when well-graded sand and fiber reinforcement is used (Shah 2017), meaning a plateau may occur that is heavily dependent only on non-cementitious ingredients.

Pozzolanic reaction rate also increase with temperature, leading to higher strength for concretes with silica fume (Maage 1984). X-ray diffraction analysis of UHPC cured at different temperatures by Prem et al. (2015) indicated that high temperatures resulted in a different microstructure. Strengths exceeding 200 MPa have been reported from specialized specimen preparation and microwave treatment (Korpa and Trettin 2008), however, implementation of these methods would bring challenges to field applications. Differing from what has been observed for UHPC, several studies have shown that curing conventional concretes and HSCs at elevated temperatures increased early age strength, but a cross-over in strength was observed after several days in which lower temperature cured specimens achieved higher strength at later ages (Carino 1984; Carino and Lew 2001; Cervera 2002; Kim et al. 1998; Lee et al. 2016).

Table 2.1 Mechanical Properties for Selected Curing Conditions

Reference	UHPC type	Curing Description	f_c or E Key Findings	
Ahmad and Hakeem 2015	UHPC premix similar to others mixed with W_f of 6.2%.	1) 28 days in 22±2°C air 2) 28 days in 22±2°C water followed by cyclic heating-cooling exposure for 6 months	f_c	Before exposure, curing 1 and 2 achieved f_c of 149 and 163 MPa, respectively. After exposure for curing 2, cylinders achieved f_c of 194 MPa.
			E	Before exposure, curing 1 and 2 achieved E of 49 and 57 GPa, respectively. After exposure for curing 2, cylinders achieved E of 62 GPa.
Alsalman et al. 2017	UHPC made from a Ductal premix with natural-gradation sand and V_f of 0, 2, 4, and 6%.	100% RH at 60°C for 2 days and 90°C for 3 days	f_c	With respect to increasing V_f, curing achieved average f_c of 133, 137, 139, and 152 MPa.
			E	With respect to increasing V_f, curing achieved E of 39, 40, 42, and 44 GPa.
Graybeal 2006	UHPC made from a Ductal premix with V_f of 2%.	1) Open air 2) 2 days steam at 90°C 3) 2 days at 60°C 4) 2 days steam at 90°C after 14 days in open air	f_c	Average 28 day f_c of 126, 193, 171, and 171 MPa for curing 1, 2, 3, and 4, respectively.
			E	Average 28 day E of 43, 52, 51, and 50 GPa for curing 1, 2, 3, and 4, respectively.
Howard et al. 2018a	UHPC made from ERDC Cor-Tuf with V_f of 3.2%.	1) 120 days in 100% RH 2) 6 days 100% RH and 7 days in 90°C bath 3) 6 days 100% RH and 8 days in 80°C bath	f_c	Average f_c values following curing 1, 2, and 3 were 149, 175, and 190 MPa, respectively.
			E	Average E values following curing 1, 2, and 3 were 49, 50, and 53 GPa.
Prem et al. 2015	Cube specimens of unique UHPC mixture with V_f of 2%.	1) 20°C water only 2) 100°C steam for 18 hours followed by water 3) 200°C heat treatment for 48 hours followed by water	f_c	Specimens were cured in 20°C after curing 2 and 3. Cubes achieved 28 day f_c of 144 MPa, 142 MPa, and 196 MPa for curing 1, 2, and 3, respectively.
Wan et al. 2016	UHPC made from a Ductal premix with no fiber reinforcement.	1) 100% RH at 28°C 2) 7 days of 100% RH at 28°C followed by 7 days in 85°C water	f_c	Average 14 day f_c of 99 and 127 MPa for respective curing conditions.
William et al. 2009	UHPC made from ERDC Cor-Tuf with V_f of 3.6%.	100% RH at 22°C followed by 4 days in 85°C water and 2 days at 85° in oven.	f_c	Average f_c of 224 MPa.
			E	Average E was 47 GPa.

-- Curing description neglects handling and demolding of specimens in first 24 hours
--W_f = fiber fraction by mixture weight, V_f = fiber fraction by mixture volume
-- RH = relative humidity

2.3 Predicting Mechanical Properties

Currently, ACI committee 318 defines an empirical relationship: $E = 4{,}700\sqrt{f_c}$ for MPa units or $E = 57{,}000\sqrt{f_c}$ for psi units (ACI 318). It is common practice to specify a required E based on this established relationship. Alsalman et al. (2017) demonstrated that the ACI 318 relationship overestimates UHPC modulus and suggested a new equation.

Predicting in-place concrete strength over time is of particular importance to the sequence of construction events, such as curing procedure and time of formwork removal. ASTM C1074 is the industry standard maturity method for predicting concrete strength and attempts to account for the time- and temperature-dependence of property development. Two alternative functions are proposed by C1074: (i) temperature-time factor, referred to as maturity in °C-days, and (ii) equivalent age. Maturity predictions assume a linear relationship between time and temperature effects on strength gain; specimens of a given mixture with the same maturity should have similar strengths. Equation 2.1 shows the formula used in this study to calculate maturity where T is the concrete temperature during time interval Δt. The datum temperature, T_0, is set to 0°C and discussed later in Chapter 5.

$$\text{Maturity}(t) = \sum(T - T_0)\Delta t \tag{2.1}$$

Different from maturity, equivalent age scales the reaction time at different temperatures to a reference temperature. Equivalent age accounts for the interaction between temperature and reaction rate, modeled with the Arrhenius equation, in which higher temperatures tend to accelerate reaction rate (Logan 1982). Specifically, the Arrhenius relationship requires an accurate determination of activation energy and chemical affinity, but no experimental methods currently exist for measuring these values

directly from concrete specimens. Carino (1984) showed that maturity-based f_c estimates are only accurate over a wide range of temperatures for concretes with low activation energy (E_a) (approximately 30 kJ/mol), while concretes with high "activation energies" (approximately 56 kJ/mol) resulted in a highly nonlinear time-temperature relationship. C1074 outlines an approximate method to determine E_a using f_c data of mortar cubes cured at different temperatures and durations, but the recommended range of temperatures – 12 to 32°C – is much narrower than temperatures often experienced by UHPC. This method is discussed in Section 5.1.

Several numerical models have been employed to relate age and concrete mechanical strength development. Models of the hyperbolic form have been used extensively to approximate concrete's relative strength gain over a range of ages with parameters fit using regression analysis (Carino 1984; Carino and Lew 2001; Habel et al. 2006; Kim et al. 1998; Kim et al. 2001; Lee et al. 2016). Equation 2.2, suggested by Carino (1984), represents this relationship; terms are denoted f_c for the compressive strength at time t, f_{lim} is the limit strength or theoretical ultimate strength after infinite curing time, k is the rate constant (1/day), and t_0 is a strength offset time corresponding to the beginning of strength development. Habel et al. (2006) showed that the hydration reaction of UHPC at ambient temperature has virtually stopped by 90 days and Wan et al. (2016) found that UHPC reached 95% of its aging degree when cured for 7 days in a 28°C moist room followed by 7 days in an 85°C water bath. The behavior of a hyperbolic strength function therefore appears even more applicable to a UHPC system because the limiting strength is approached much sooner than for conventional concretes. ACI Committee 209

recommends a strength development formula similar to Equation 2.2 that is also of the hyperbolic form (ACI 209).

$$f_c = f_{lim} \frac{k(t-t_0)}{1+k(t-t_0)} \; for \; t \geq t_0 \tag{2.2}$$

For Equation 2.2 to account for curing temperature, individual terms (e.g., f_{lim} and k) can be expressed as functions of temperature. Multiple studies have replaced time with equivalent age, making use of the Arrhenius function, and replace k with an equivalent rate at the reference temperature (Habel et al. 2006; Carino 1984; Carino and Lew 2001; Kim et al. 1998; Kim et al. 2001; Lee et al. 2016). The accuracy of these models' predictions are dependent on the selection of E_a and other input parameters. Studies have attempted to determine an accurate representation of E_a for concrete at different temperatures (D'Aloia and Chanvillard 2002; Kim et al. 2001). Although results of predictive modeling were improved, Kim et al. (2001) recognized that E_a changes over time and that mechanical measurements at late ages of 90 and 365 days were required to achieve a decent fit, which is not always feasible.

2.4 Full-Scale Simulations

Conventional concrete has been shown to increase in temperature considerably when large volumes of concrete retain chemically released heat during hydration (Gajda 2007). With higher cement content, these thermal effects are more likely to develop in UHPC. Andersen et al. (1994) developed an incremental finite element analysis for concrete structures that optimizes the construction sequence considering the development of temperature, materials properties, thermal strains, and nonlinear effects including creep and shrinkage. Similarly, Fairbairn et al. (2004) developed an incremental framework that

optimized the construction of a concrete, hydroelectric dam. Parameters of this model included the concrete material properties, temperature development, sequence/duration of construction events, construction cost, and a method to determine the risk of cracking. Development of mechanical properties was represented using a hydration model from Ulm and Coussy (1995) that accounts for both temperature and moisture. Simulations were performed iteratively to determine the optimal balance of construction cost, scheduling, and mechanical property development. Both models by Andersen et al. and Fairbairn et al. took into consideration how the temperature history affects development of mechanical properties and thermal stresses.

Complex numerical frameworks have been developed to couple the contribution of thermodynamics and moisture transport on the kinetics of cement hydration. Instead of fitting functions of time to collected strength data, these frameworks utilize theoretical relationships to represent the chemical reactions within concrete and factors affecting them. Mechanical property development has been related to hydration reaction state for conventional concrete (Cervera et al. 1999; Cervera et al. 2002; Faria et al. 2006; Ulm and Coussy 1995) and extended to HSC and UHPC (Wan et al. 2016; Di Luzio and Cusatis 2009). These coupled models depend on many input parameters and are intended for implementation in fairly sophisticated finite element analysis routines. Determination of some input parameters are not standard construction practice and requires a fair amount of guesswork for successful implementation.

Numerical strength models attempt to predict an experimentally-measured quantity (e.g. f_c), but most of the models discussed depend on properties that are difficult to measure and/or relate to a physical phenomenon. As the interaction of constituents and curing

regimes becomes more complex, such as with UHPC, use of standard testing methods as the basis for predictive modeling efforts should be considered.

CHAPTER III

EXPERIMENTAL PROGRAM

A dataset was prepared which captures time- and temperature-dependent f_c and E values under specific laboratory curing conditions. A total of 475 specimens were prepared for this study, partitioned between isothermal and mixed temperature conditions. All specimens were prepared using the same set of raw materials and mix proportions (Table 3.1) and constitute the Cor-Tuf UHPC mixture developed by ERDC.

Table 3.1 Ingredient Properties and Proportions of Cor-Tuf Mixture

Constituent	Specific Gravity	Description	Batching Quantities for 0.14 ft^3 (0.00396 m^3)
Air	0.00	Air Filling Voids in UHPC	-
Water	1.00	Taken from Laboratory Tap	1.46 lb.
Steel Fibers	7.85	Dramix® 3D 55/30 BG	2.10 lb.
Admixture	1.08	ADVA® 190	49.4 ml
Cement	3.15	API Class H (HSR) Cement	6.90 lb.
Silica Fume	2.25	Elkem Microsilica ES 900-W	2.70 lb.
Silica Flour	2.65	SIL-CO-SIL® 75 Ground Silica	1.90 lb.
Sand	2.65	F-50 Whole Grain Silica	6.70 lb.

3.1 Specimen Preparation

Ingredients were batched to produce 0.14 ft^3 (3.96×10^{-3} m^3) of fresh UHPC for two 4 inch by 8 inch (10.2 cm by 20.3 cm) cylinders. Dry ingredients were placed into the bowl of a 20 quart high-shear, table top mixer. Dry ingredients were blended on the lowest mixer setting for approximately 60 seconds. Then, 80% of the total water was added and mixed

for 90 seconds. Next, admixture and the remaining water were added. Mixing then continued in five minute intervals, pausing between intervals to remove dry materials from the edges of the bowl and paddle attachment. The ingredients were mixed until reaching a fluid, self-consolidating consistency. Thereafter, fibers were added and mixed until evenly dispersed. The resulting mixture was placed into two cylindrical molds in two lifts. Consolidation to remove air was performed with a vibrating table (used for 2 minutes after each lift) instead of the rodding method which can alter random fiber orientation. Fabricated specimens were covered with a plastic bag to prevent water evaporation. Specimens were then cured as discussed in the following sections prior to testing.

3.2 Curing

Five curing environments were used in this study (Figure 3.1): lab bench, curing room, and water baths (room-temperature, cooled, and heated). The covered specimens were placed on a general-use lab bench (Figure 3.1a) for their first day of curing and the temperature of this location was monitored intermittently. A 100% relative humidity curing room (Figure 3.1b) was maintained at 23°C ±2°C as per ASTM C192 (temperature was monitored using a data logger). Plastic bins were filled with water and maintained at room temperature (Figure 3.1c). Two cooling tanks were used for specimens cured at a temperature of 10°C (Figure 3.1d). Stainless steel water baths were used to cure specimens at elevated temperatures (Figure 3.1e). The temperature of each bath was checked intermittently using a hand-held, digital thermometer. Water baths in Figure 3.1.c to 3.1.e were saturated with hydrated lime according to ASTM C511 (2013).

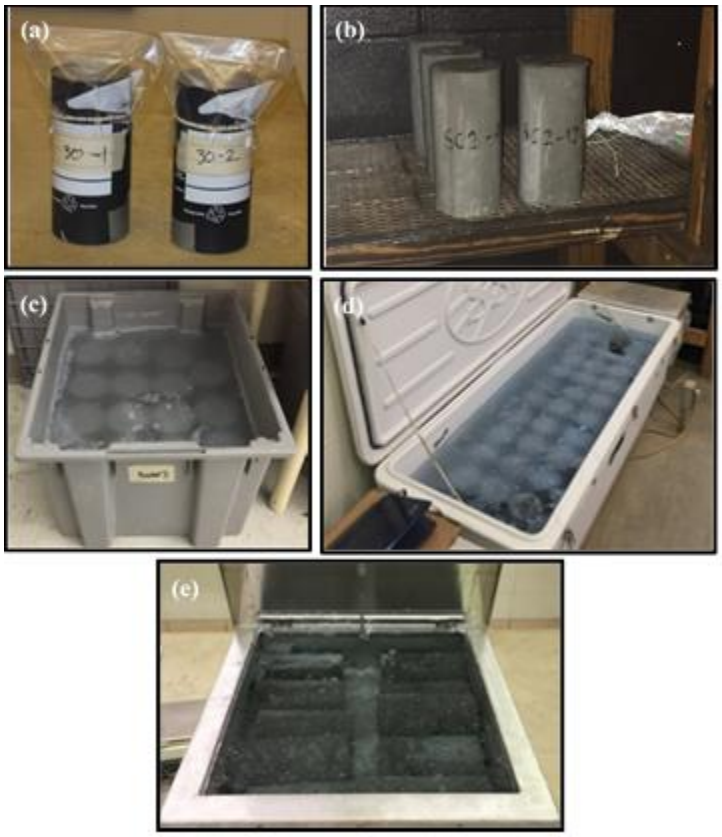

Figure 3.1 Depiction of the five curing environments

(a) lab bench, (b) curing room, (c) room-temperature bath, (d) chilled bath, and (e) heated bath.

The term “isothermal conditions” is used herein to generalize constant temperature curing once a cylinder is removed from its mold. A total of 404 specimens were cured under isothermal conditions designated by a prefix “I” followed by a number representing the constant curing temperature in degrees Celsius (e.g. I30 is at 30°C). For isothermal specimens cured in a moist room, the curing group designation is followed by the letter “M.” Cylinders placed in water baths were cured at constant temperatures of 10, 23, 30, 50, 70, and 90°C. All specimens remained in their curing group until the designated testing

time. To characterize the development of mechanical properties as a function of time and temperature, curing durations were targeted using increments of maturity as defined by ASTM C1074. Further details for maturity calculations can be found in Howard et al. (2018b). Table 3.2 outlines the number of specimens per curing group and the range of maturities considered. I10, I23, and I23M cylinders were removed from curing approximately every 40°C-days, which resulted in 60 specimens per group. I30, I50, I70, and I90 cylinders were removed from curing approximately every 50°C-days, which resulted in 42 specimens per group. Additional specimens were added to some groups to provide more resolution at early ages.

Table 3.2 Isothermal Curing Ranges

Curing Group	Curing Temp.	Curing Environment	n	Start		End	
				Maturity (°C-days)	Age (days)	Maturity (°C-days)	Age (days)
I10	10°C	Lime Bath	70	54	4.0	2557	251
I23	23°C	Lime Bath	77	16	0.7	2332	111
I23M	23°C	Moist Room	71	16	0.8	2522	109
I30	30°C	Lime Bath	43	99	3.7	2151	72
I50	50°C	Lime Bath	50	38	1.3	2148	44
I70	70°C	Lime Bath	43	98	2.2	2146	32
I90	90°C	Lime Bath	50	32	1.2	2142	25

-- n = number of specimens

A total of 72 specimens were cured under mixed temperature conditions. Five mixed temperature conditions were used, denoted as M2, M6, M13, M20, and M27. After one day on the lab bench, specimens were placed into the moist curing room for a specified duration of time, followed by seven days in a 90°C water bath. For conditions M2, M6, M13, M20, and M27, the specified duration in the curing room was 2, 6, 13, 20, and 27

days, respectively. Of the 72 specimens, 62 were used to evaluate the effects of multiple temperature conditions, designated as category M. The remaining 10 specimens were tested to evaluate the effect and variability of specimen temperature on E. These specimens, denoted by category V, were cured according to condition M6. Curing condition M6 is identical to a curing procedure recommended by ERDC that has been used in previous research efforts at MSU (Howard et al. 2018a). To assess the variability of this method, 30 specimens received M6 designation. The other four conditions (M2, M13, M20, and M27) investigated the mechanical properties as a function of duration in the curing room before high temperature exposure. Eight specimens were each allocated to the M2, M13, M20, and M27 groups.

3.3 Mechanical Testing

Prior to testing, ends of specimens were ground smooth using a cylinder end grinder (Figure 3.2a). For selected specimens, densities were determined using calipers and a digital scale. After curing, isothermal specimens were prepared for testing as quickly as possible so that each specimen was tested very closely to its curing temperature, while M and V specimens were cooled to room temperature. After room temperature testing, all 10 V specimens were conditioned at 10, 50, and 90°C to determine E at temperatures near the conditioned temperature. Compressive strength and elastic modulus testing were conducted according to ASTM C39 and C469, respectively. The only deviation from ASTM requirements was for I and V specimens that were not tested at room temperature. Compression testing is shown in Figure 3.2b.

Elastic modulus deflections were measured in one of two ways: (i) an analog dial (Figure 3.2c), and (ii) a linearly variable displacement transducer (LVDT) (Figure 3.2d).

All I and M specimens were tested using the analog dial. Elastic modulus of category V specimens was conducted at room temperature with the analog dial twice and LVDT twice to compare results between both methods. Subsequent tests at 10, 50, and 90°C were performed using the LVDT. The average E for dial (E_{dial}) and LVDT (E_{LVDT}) methods at room temperature were compared for V specimens and found to be statistically similar. A paired, two-tailed t-test returned a p-value of 0.81, indicating that results from both methods are comparable.

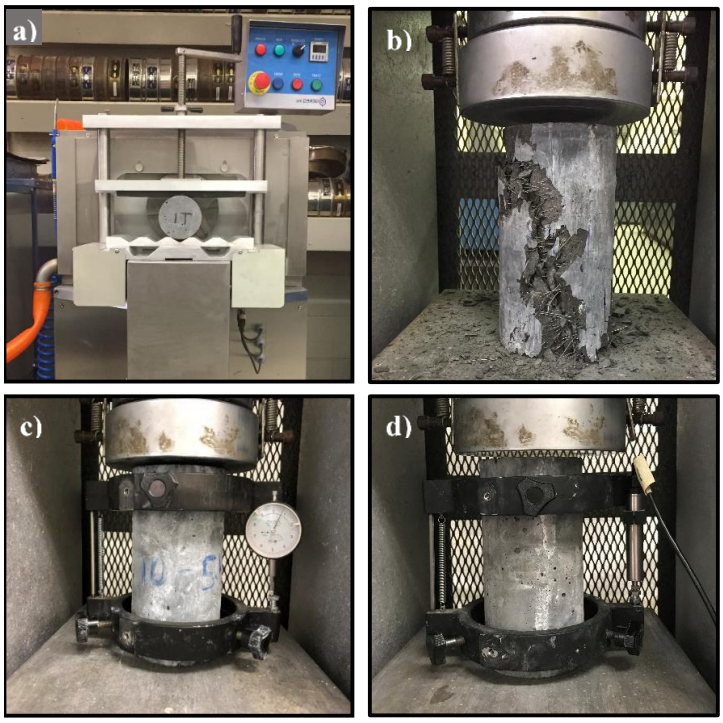

Figure 3.2 Mechanical Testing Equipment

a) end grinder; b) specimen after compression test; c) specimen in compressometer with analog dial; d) specimen in compressometer with LVDT

CHAPTER IV

EXPERIMENTAL RESULTS

4.1 Elastic Modulus versus Temperature Results

Results of E versus temperature for category V cylinders are presented in Figure 4.1. Values are averaged over all 10 cylinders at each testing temperature using the LVDT method. A strong linear relationship between E and specimen temperature is observed. Based on these results, a temperature correction is proposed in Equation 4.1 where E is the elastic modulus as measured, T denotes the temperature of curing or conditioning in degrees Celsius, and E_{23} is the measurement adjusted to 23°C.

$$E_{23} \cong E + 0.0805 * (T - 23°C) \quad (4.1)$$

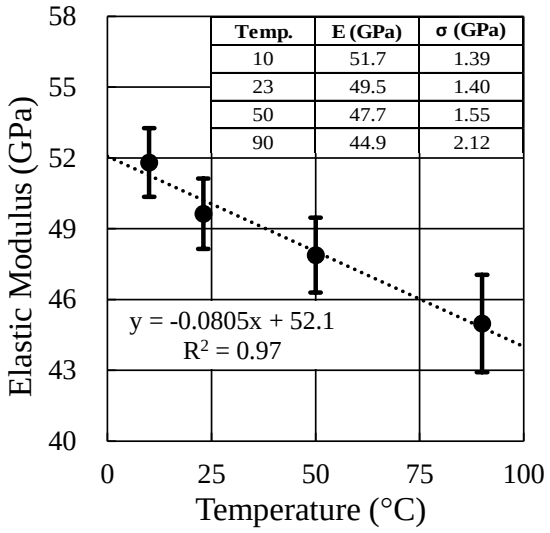

Figure 4.1 Temperature Sensitivity of Elastic Modulus Results

4.2 Isothermal Curing Temperature Effects

Raw data for category I cylinders are provided in appendix Tables A.1 through A.7. Table 4.1 summarizes isothermal f_c over two ranges of maturities and E after 1000°C-days with statistics including average (μ), standard deviation (σ), and number specimens (n). The E_{23} values do not appear to follow a linear trend with curing temperature and the average E_{23} for I23M and I50 is much lower than other curing groups.

Table 4.1 Isothermal Curing Mechanical Results at Selected Maturity Ranges

Curing Group	f_c 400-600°C-days			f_c 1900-2100°C-days			E_{23} ≥ 1000°C-days		
	μ (MPa)	σ (MPa)	n	μ (MPa)	σ (MPa)	n	μ (GPa)	σ (GPa)	n
I10	124.3	10.5	5	146.6	5.0	5	52.43	1.6	9
I23	132.2	5.4	4	157.9	6.1	5	51.60	1.3	9
I23M	125.8	3.4	4	137.0	4.7	5	46.17	1.5	9
I30	145.6	10.6	4	158.5	6.6	4	50.98	1.7	7
I50	153.1	8.2	4	150.1	5.7	5	48.97	0.6	7
I70	164.7	6.6	4	166.3	13.6	4	52.20	1.5	7
I90	168.6	11.4	4	177.5	20.5	4	53.98	0.7	7

Comparisons between measured E values and E_{23} from Table 4.1 are shown in Figure 4.2. Figure 4.2.a shows that the measured E values follow a somewhat quadratic trend. Lower temperature curing appears to yield higher stiffness, but these same specimens were tested at lower temperatures. It is known that elastic modulus of many materials decreases with increasing temperature, so the temperature of the elastic modulus test itself may be affecting the trend. This observation is the initial reason V specimens were added to the experimental program to separate the effect of testing temperature from curing temperature and develop Equation 4.1. Figure 4.2.b displays these values adjusted to E_{23} and shows a quadratic trend with a minimum around 50°C. The I50 specimens were left on the lab bench 12 hours longer than other curing groups, so their properties may be affecting trends slightly. Figure 4.2.c shows the E_{23} results again, but I50 data is excluded. The resulting quadratic fit has a higher R^2 than Figures 4.2.a or 4.2.b and still predicts a minimum near 50°C. As such, numerical modeling efforts will reflect these trends, discussed in Chapter V.

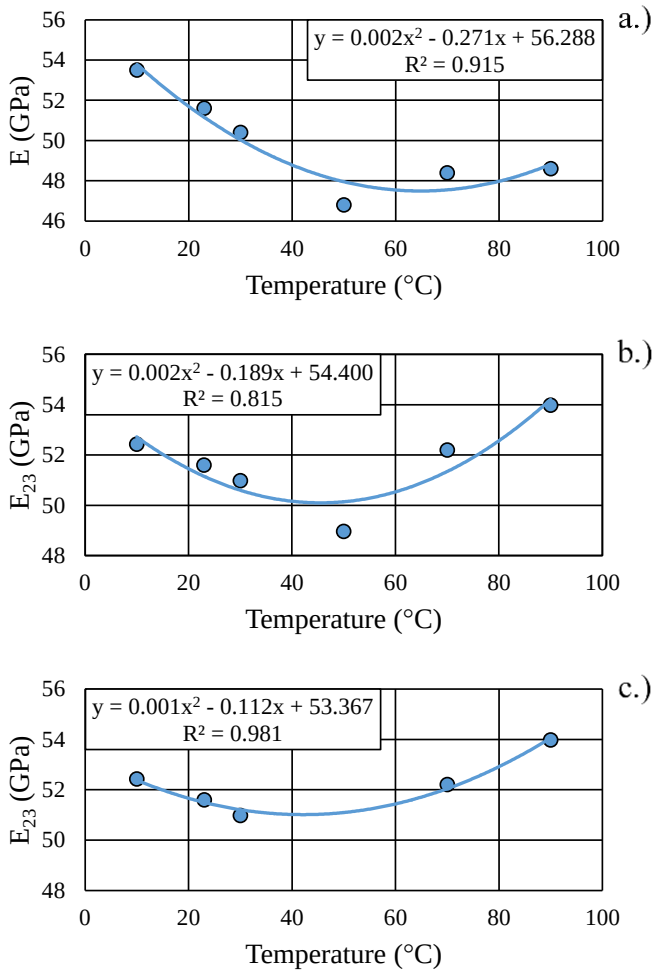

Figure 4.2 Average E and E_{23} versus Temperature after 1000°C-days

a.) Measured elastic modulus values, b.) Adjusted modulus values, and c.) Adjusted modulus values excluding I50.

Figure 4.3 presents all E_{23} results for I10, I23, I30, I50, I70, and I90 cylinders plotted against maturity. Most cylinders recorded a modulus near 50 GPa regardless of curing temperature after maturities of 500°C-days, similar to values reported in literature (Ahmad and Hakeem 2015; Graybeal 2011; Howard et al. 2018a). At maturities less than 500°C-days, higher temperature curing groups have equal or higher stiffness than lower

temperature curing, indicating that higher temperature cured specimens developed stiffness in less time.

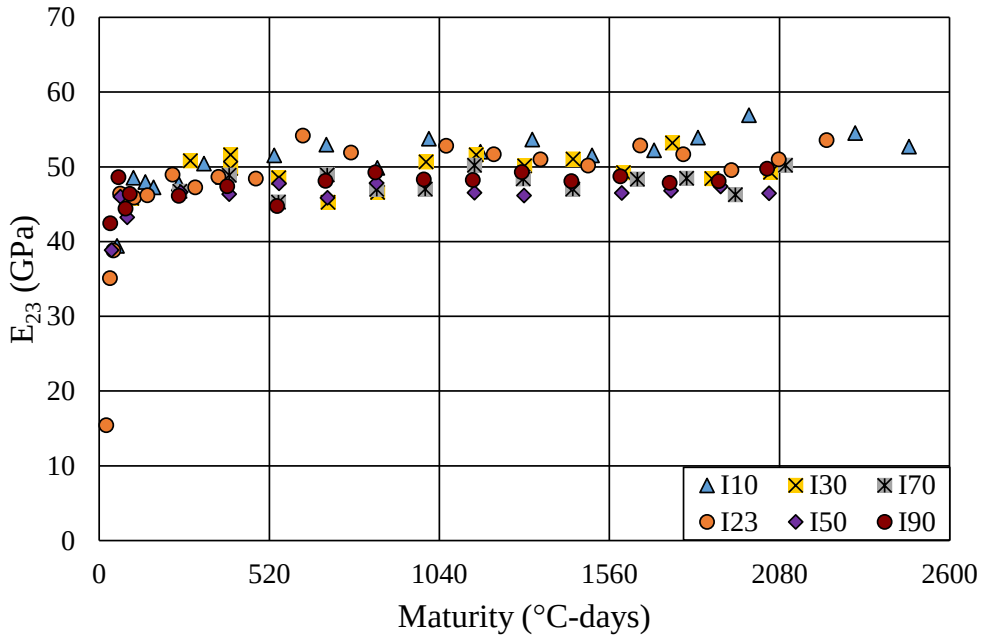

Figure 4.3 Elastic Modulus Results for Isothermal Curing

Compressive strength results for I10, I23, I30, I50, I70, and I90 cylinders are plotted against maturity in Figure 4.4. In general, higher temperature curing conditions yielded higher f_c than for colder conditions at a given maturity. It is not believed that temperature effects are significantly changing the f_c results in the same way that modulus is affected, although it is difficult to verify in the same way as elastic modulus since a specimen cannot be retested after the compressive strength is determined. Ongoing research efforts plan to validate the accuracy of the previous statement, but is not contained in this thesis.

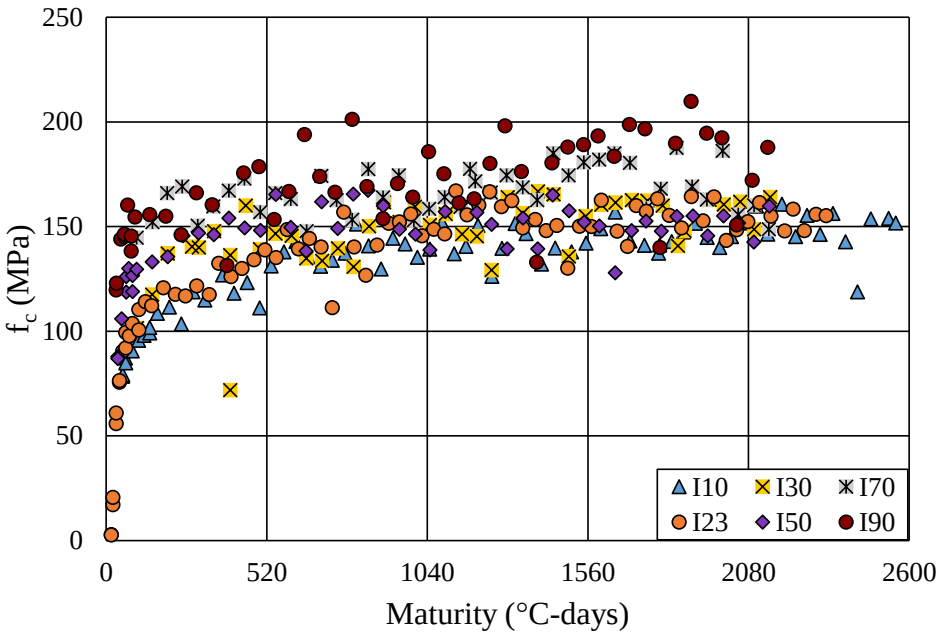

Figure 4.4 Compressive Strength Results for Isothermal Curing

Values in Table 4.1 show the general trend that f_c increases with curing temperature for both maturity ranges. At 1900-2100°C-days, variability appears to be highest for I70 and I90 curing groups, which is evident in Figure 4.4.

Figure 4.5 shows paired E and f_c results of category I and M specimens. ACI committee 318 defines a relationship between E and the square root of f_c multiplied by a constant of 4700 in units of MPa (57,000 in units of psi) (ACI 318). Equation 4.2 shows this general relationship for a constant denoted C_{469} according to the ASTM test method for elastic modulus.

$$E = C_{469}\sqrt{f_c} \tag{4.2}$$

As seen in Figure 4.5, the ACI constant value of 4700 over predicts the modulus for most f_c. Regression with Equation 4.2 yielded best fit constant, C_{469}, of 4170 for all I and M specimens, indicating that Cor-Tuf develops disproportionately higher f_c than E.

This trend is shown in Figure 4.5 with a resulting R^2 of 0.73. Best fit constants were also determined for isothermal groups individually. For groups I10, I23, I30, I50, I70, and I90, the resulting C_{469} constants were 4416, 4270, 4167, 3972, 3971, and 4118, respectively, indicating a trend with temperature. The equation proposed by Alsalman et al. (2017) is also shown in Figure 4.5 with an R^2 of 0.56.

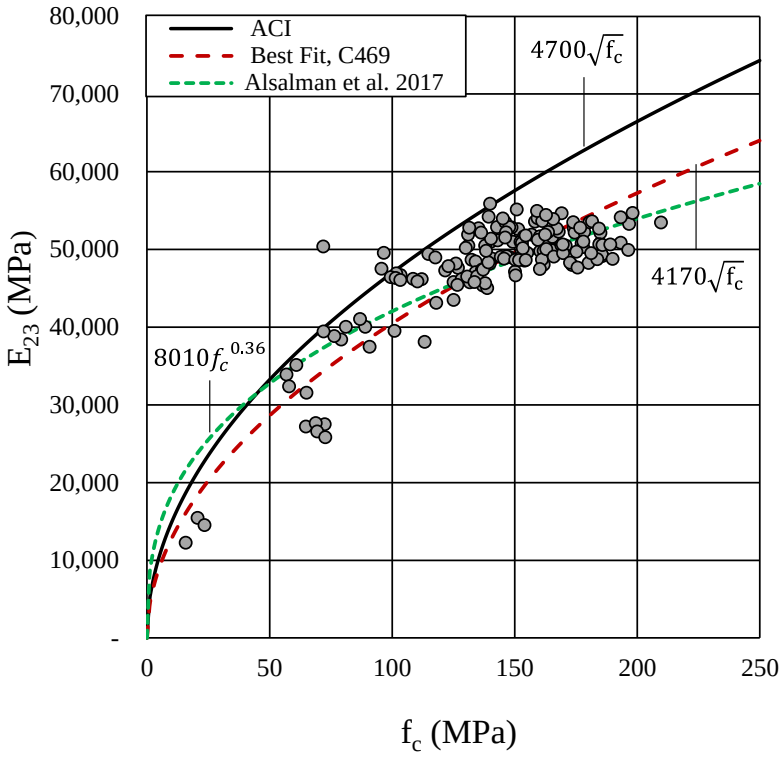

Figure 4.5 Compressive Strength versus Elastic Modulus for I and M Cylinders

4.3 Isothermal Curing Moisture Effects

Figure 4.6 compares I23 and I23M curing methods using equality plots. Figure 4.6.a shows f_c of I23 and I23M specimens at the same ages and maturities. Although these cylinders were cured at the same temperature for the same durations, the lime-water bath shows an 11% increase in strength (according to linear regression), highlighting the

importance of moisture availability for strength gain. Additionally, only 7 of the 71 data points in Figure 4.6.a lie below the equality line, confirming the general increase in strength associated with the lime-water bath.

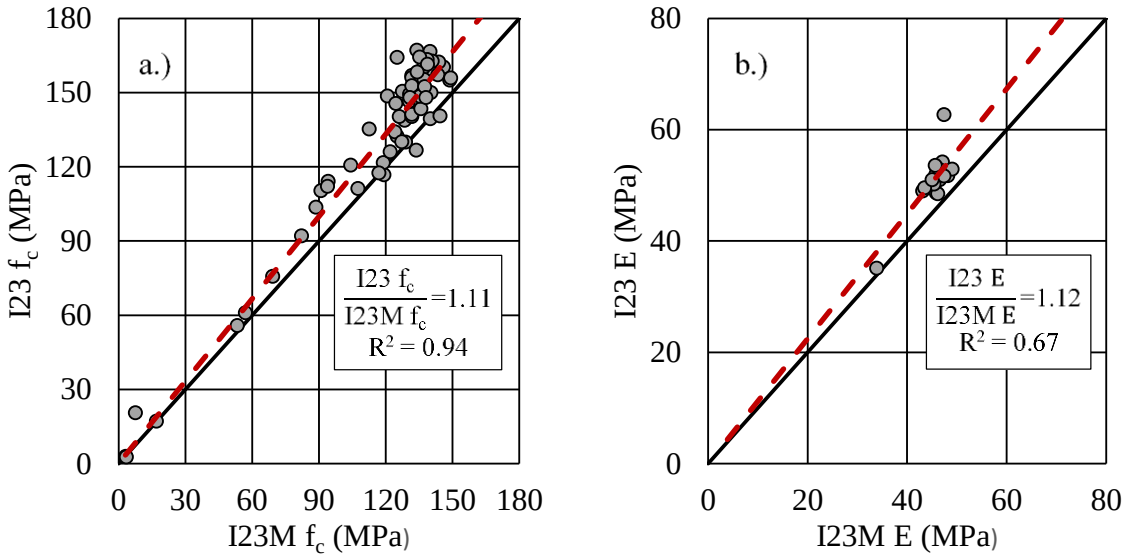

Figure 4.6 Compressive Strength and Elastic Modulus Equality Plots for I23M and I23 Cylinders

Similarly, Figure 4.6.b shows 16 E pairs of I23 and I23M specimens. As discussed in Section 3.3, modulus was measured on every fourth specimen. Elastic modulus of I23 and I23M specimens were collected at staggered times, but with same interval of time in between consecutive modulus tests. The average age of I23 specimens is 1.4 days younger than its corresponding I23M specimen for E comparison in Figure 4.6.b. Similarly, the average maturity is 31.6°C-days less for I23 compared to I23M. Even though the modulus of I23M specimens was always collected at a later age than I23, a very similar trend to f_c is observed indicating that I23 specimens are 12% stiffer than I23M. For all 16 pairs, I23 reported a higher modulus than I23M. Compared to moist curing at 23°C, submerged water

bath curing yielded 11% higher f_c and 12% higher E at both early and late ages. These trends are surprisingly consistent and could easily be implemented in the numerical model developed in Chapter V.

4.4 Mixed Curing Results

Results for category M specimens are summarized in Table 4.2. Statistics for f_c and E include average (μ), standard deviation (σ), coefficient of variation (COV), and number of specimens (n). For f_c, M6 curing provides the highest average strength followed by M2. The other groups (M13, M20, and M27) did not result in significantly higher strength despite the longer curing duration compared to M2 and M6. Groups M2 and M6 achieved similar to the average I90 f_c for maturities 1900-2100°C-days (shown in Table 4.1), despite M2 and M6 having maturities of 698 and 791°C-days, respectively. While the I group indicates that f_c increases with temperature, the M group suggests that delaying heat exposure may benefit development of strength. Average E values do not appear to differ meaningfully with a range of only 1.3 GPa, which implies that E is not affected by curing temperature to the same degree as f_c.

Table 4.2 Mixed Curing Results

Group	Age (days)	Maturity (°C-days)	f_c				E			
			μ (MPa)	σ (MPa)	COV	n	μ (GPa)	σ (GPa)	COV	n
M2	10.0	698	175.4	13.1	7.5%	8	50.4	3.3	6.5%	4
M6	14.1	791	179.2	10.3	5.7%	30	50.3	2.0	4.0%	15
M13	21.1	955	151.9	7.9	5.2%	8	50.5	5.5	10.9%	4
M20	28.0	1111	167.9	12.6	7.5%	8	49.5	1.2	2.5%	4
M27	35.0	1273	171.4	11.3	6.6%	8	50.8	1.0	1.9%	4

-- n = number of specimens

CHAPTER V

ISOTHERMAL MODEL DEVELOPMENT

A numerical model is proposed that predicts the f_c and E development of Cor-Tuf UHPC cylinders cured under isothermal conditions. The general relationship used in this study is the hyperbolic expression proposed by Carino (1984) for isothermal curing conditions given in Equation 2.2. This chapter describes numerical analyses conducted to evaluate the most appropriate model formulation. First, the provisions of ASTM C1074 are investigated to evaluate its applicability to the isothermal data set. Then, the numerical model is formulated with selected parametric functions.

5.1 ASTM C1074 parameters for Isothermal Curing Data

This section explores the procedures suggested in the Appendix of ASTM C1074 titled "Determination of Datum Temperature or Q-Value." C1074 uses the same hyperbolic equation suggested by Carino (1984). C1074 requires compressive strength of mortar cubes cured at three different temperatures to be fit to the hyperbolic equation by finding values for the limit strength, rate term, and offset term that minimize the square of the errors. Strengths are supposed to be collected at 1, 2, 4, 8, 16, and 32 days. Although mortar cubes were not prepared according to C1074 for this study, the strength data for category I cylinders was analyzed. Similar to the fitting procedure described more thoroughly in Section 5.2, the terms f_{lim}, k, and t_0 were fit for each of the 6 curing groups. No terms were

described by parametric functions of time or temperature and each curing group was fit separately. The offset term was constrained to always be equal to greater than 0. Resulting terms are shown in Table 5.1.

Table 5.1 Hyperbolic terms fit for ASTM C1074

Curing Group	f_{lim} **(MPa)**	k **(1/day)**	t_0 **(days)**
I10	147.5	0.204	0.00
I23	153.3	0.576	0.66
I30	158.2	0.724	1.03
I50	153.3	3.802	0.97
I70	172.1	2.752	0.00
I90	183.1	2.048	0.00

ASTM C1074 describes the terms Q and T_0 which are inputs into the equivalent age formula. T_0 is the datum temperature which is intended to approximate the temperature below which cement hydration will cease. Carino (1984) shows this term Q is equal to the activation energy, E_a, divided by the gas constant R. As mentioned previously, activation energy has been the subject of several studies for understanding the role temperature has on the rate of hydration and strength gain. In order to determine the value of Q, the procedure in C1074 says to plot the natural logarithm of the fit *k* values versus the inverse of curing temperature in Kelvin. The negative of the slope of the best fit line is Q. Similarly, the datum temperature T_0 is found by plotting rate constant, *k*, versus the curing temperature in Celsius. The intercept with the time axis of the best fit line is the datum temperature. Figures 5.1.a and 5.1.b show these two plots.

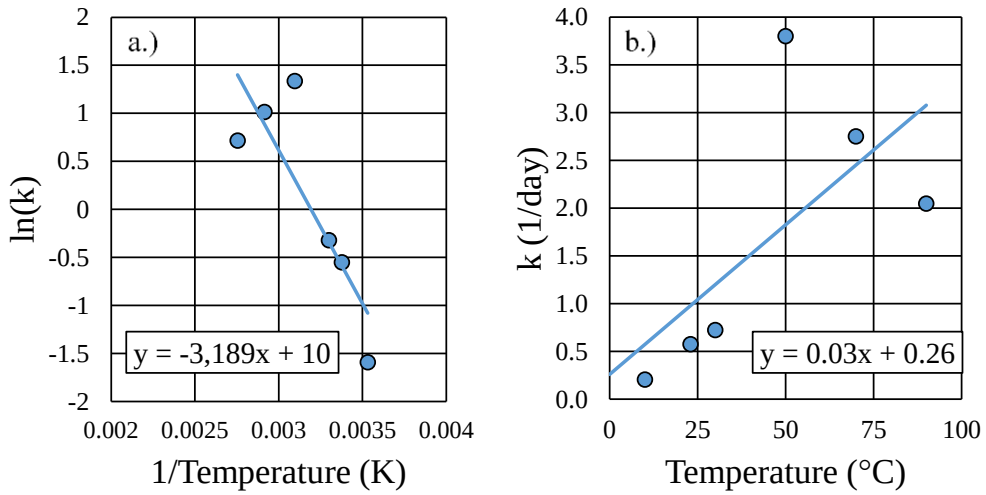

Figure 5.1 Determination of ASTM C1074 Variables for all Curing Temperatures a.) Activation energy; and b.) Datum temperature

Based on the slope of the line in Figure 5.1.a and a gas constant of $8.314*10^{-3}$ kJ/K-mol, the calculated activation energy is 26.5 kJ/mol which is a low value according to Carino. Based on the trend line in Figure 5.1.b, the calculated datum temperature is -8.3°C. The fit values for rate constant *k* does not trend with temperature well for either plot in Figure 5.1. Fit values corresponds to 10, 23, and 30°C do appear to follow a linear trend, but this is not followed by higher temperatures. A sudden increase in *k* occurs at 50°C, but then decreases again.

The procedure outlined by ASTM C1074 only uses three temperature to cure mortar cube specimens. The three curing temperatures in the example contained in the Appendix of C1074 are 12, 23, and 32°C. The determination of E_a and T_0 are performed again using only the isothermal data for 10, 23, and 30°C. Figure 5.2 shows the resulting plots. In this case, the resulting E_a and T_0 are 46.7 kJ/mol and 0.5°C, respectively. This E_a is

considerably higher than previously calculated. The datum temperature has also increased considerably. Both linear trend lines appear to agree well with the truncated data.

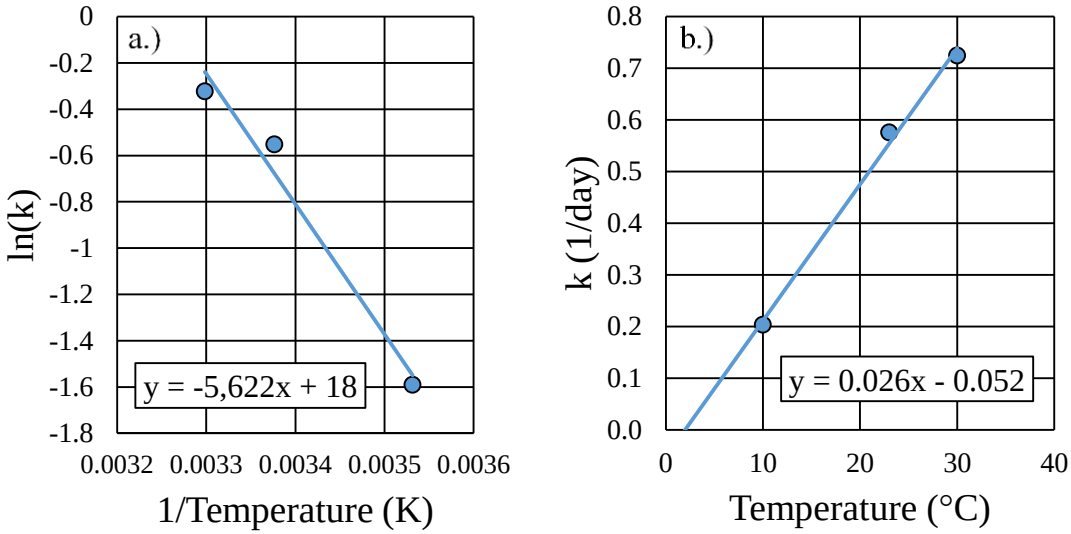

Figure 5.2 Determination of ASTM C1074 variables for 10, 23, and 30°C
a.) Activation energy; and b.) Datum temperature

These results show that provisions in ASTM C1074 for determining the activation energy and datum temperature are not applicable to this dataset. Successful implementation of equivalent age and maturity functions for predicting strength hinge on the accuracy of these inputs. Carino (1984) shows that maturity estimates will be more accurate for lower activation energy and higher activation energy corresponds to a nonlinear relationship between temperature and reaction rate, but the significantly different E_a values found in this section make it difficult to evaluate how UHPC behaves. However, there certainly appears to be a nonlinear relationship between *k* and temperature, shown in Figure 5.1.

Maturity calculations in this thesis use a datum temperature of 0°C. This T_0 appears to be the best choice since there was closer agreement of the trend in Figure 5.2.b compared to Figure 5.1.b corresponding to T_0 values of 0.5°C and -8.3°C, respectively. Setting T_0 to 0°C provides simplicity in maturity calculations which is used in this thesis mainly as a relative measure of age.

5.2 Numerical Model Development

For this model, compressive strength and elastic modulus are analyzed separately with each term of Equation 2.2 described by different parameters functions. Elastic modulus data considered in this analysis has been adjusted with Equation 4.1, therefore, predictions are for E_{23}. A regression analysis was performed, minimizing the difference between experimental measurements and predicted values by changing parameters that describe the terms of Equation 2.2. Only data for category I cylinders cured in lime-water baths are considered in this analysis.

As shown in Figure 4.4, specimens cured at higher temperatures had higher f_c than lower temperatures at a given maturity. The limit term in Equation 2.2, f_{lim}, represents the mechanical property achieved after infinite curing time. For f_c prediction, it was assumed that the limit strength is a linear function of curing temperature. For E_{23} prediction, it was assumed that the limit modulus, E_{lim}, is a quadratic function of curing temperature. The offset term, $t_{0,}$ is closely related to the set time and the occurrence of initial f_c gain.

The rate term, k, is treated as a descending power function, as shown in Equation 5.1, to reflect that early UHPC strength gain occurs more rapidly than later ages. This rate function depends on both time and temperature. Quadratic functions of temperature are

used to represent *a(T)* and *b(T)*. For Equation 5.1 to remain positive and decrease with time, functions *a(T)* and *b(T)* must be positive for all curing temperatures.

$$k(t,T) = a(T) * t^{-b(T)} \; for \; t \geq t_0 \tag{5.1}$$

Best fit coefficients are determined using the Nelder-Mead Simplex algorithm implemented in Python (Rossum 1995) using the minimization function in the SciPy package (Oliphant 2007). Index *i* indicates a data point in a curing group, indicated by index *j*. The number of specimens in a curing group is denoted n_j. The total number of data points is denoted N. For each curing group, the root mean square percent error (RMSPE) was determined between predicted and measured values, calculated according to Equation 5.2. Mean absolute percent error (MAPE) is also calculated for statistical comparisons, shown in Equation 5.3. An objective function (Equation 5.4) was defined as the weighted average RMSPE for all curing temperatures and was simultaneously minimized for all data by iteratively changing coefficient values until error minimization was achieved. Similar to Carino (1984), it was assumed that concrete temperatures were equal to curing temperatures for all ages.

$$\text{RMSPE}_j = \sqrt{\frac{1}{n_j}\sum_{i=1}^{n_j}\left(\frac{predicted_i - measured_i}{measured_i}\right)^2} \tag{5.2}$$

$$\text{MAPE}_j = \frac{1}{n_j}\sum_{i=1}^{n_j}\left|\frac{predicted_i - measured_i}{measured_i}\right| \tag{5.3}$$

$$\text{Objective} = \left(\frac{n_j}{N}\right) RMSPE_j \tag{5.4}$$

Table 5.2 summarizes the parametric functions selected for this study and Table 5.3 shows the resulting fit coefficients. First, the numerical model is calibrated for f_c by simultaneously fitting coefficients c_0 through c_8. Then, E is fit with coefficients d_0 through

d_8 using the offset term, t_0, fit for f_c data. It is worth noting that either E or E_{23} data can be input into this analysis procedure and be predicted successfully.

Table 5.2 Numerical Model Parametric Functions

Equation	Compressive Strength, f_c	Elastic Modulus, E_{23}
Hyperbolic Model	$f_c(t,T) = f_{lim}(T)\frac{k_f(t,T)(t-t_0)}{1+k_f(t,T)(t-t_0)}$	$E_{23}(t,T) = E_{lim}(T)\frac{k_E(t,T)(t-t_0)}{1+k_E(t,T)(t-t_0)}$
Limit Term	$f_{lim}(t,T) = c_0 + c_1 T$	$E_{lim}(t,T) = d_0 + d_1 T + d_2 T^2$
Rate Term	$k_f(t,T) = a_f(T)t^{-b_f(T)}$	$k_E(t,T) = a_E(T)t^{-b_E(T)}$
Rate Parameters	$a_f(T) = c_2 + c_3 T + c_4 T^2$ $b_f(T) = c_5 + c_6 T + c_7 T^2$	$a_E(T) = d_3 + d_4 T + d_5 T^2$ $b_E(T) = d_6 + d_7 T + d_8 T^2$
Offset Term	$t_0 = c_8$	$t_0 = c_8$

Table 5.3 Resulting Fit Coefficients for Isothermal Model

Compressive Strength		Elastic Modulus	
c_0	160.2	d_0	57.5
c_1	2.53E-01	d_1	-2.89E-01
c_2	3.33E-01	d_2	2.75E-03
c_3	1.19E-01	d_3	3.40E-03
c_4	4.93E-04	d_4	-7.08E-04
c_5	4.90E-01	d_5	3.16E-03
c_6	-2.88E-03	d_6	1.31E-01
c_7	3.35E-05	d_7	-2.18E-03
c_8	7.45E-01	d_8	4.79E-05

Figure 5.3 presents the experimental data, model predictions, and fit statistics for f_c of curing groups I10, I23, I30, I50, I70, and I90. The model shows reasonable agreement with the experimental data with MAPE ranging from 4.3% to 7.7% and RMSPE ranging from 5.9% to 11.5% for different curing groups. I50 data appears to be over predicted at later ages. High variability is apparent for I90 specimens with measured values scattering

below 150 MPa and above 200 MPa, but the predicted trend agrees well with the overall dataset. The predicted limit strength is directly proportional to curing temperature, which also agrees with the experimental results in Table 4.1. Similarly, Figure 5.4 presents the experimental data, model predictions, and fit statistics of elastic modulus for the same curing groups as Figure 5.3. The regression analysis indicates good agreement between the model predictions and experimental data with MAPE ranging from 1.8% to 6.0% and RMSPE ranging from 2.7% and 10.2%.

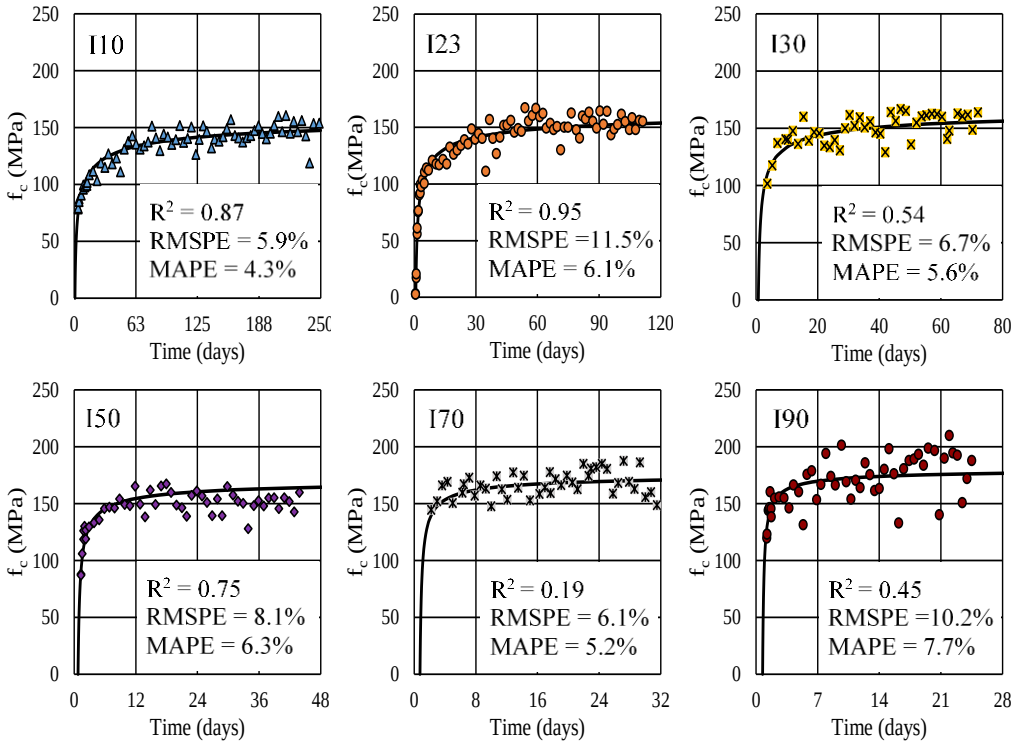

Figure 5.3 Compressive Strength Measurements and Predictions

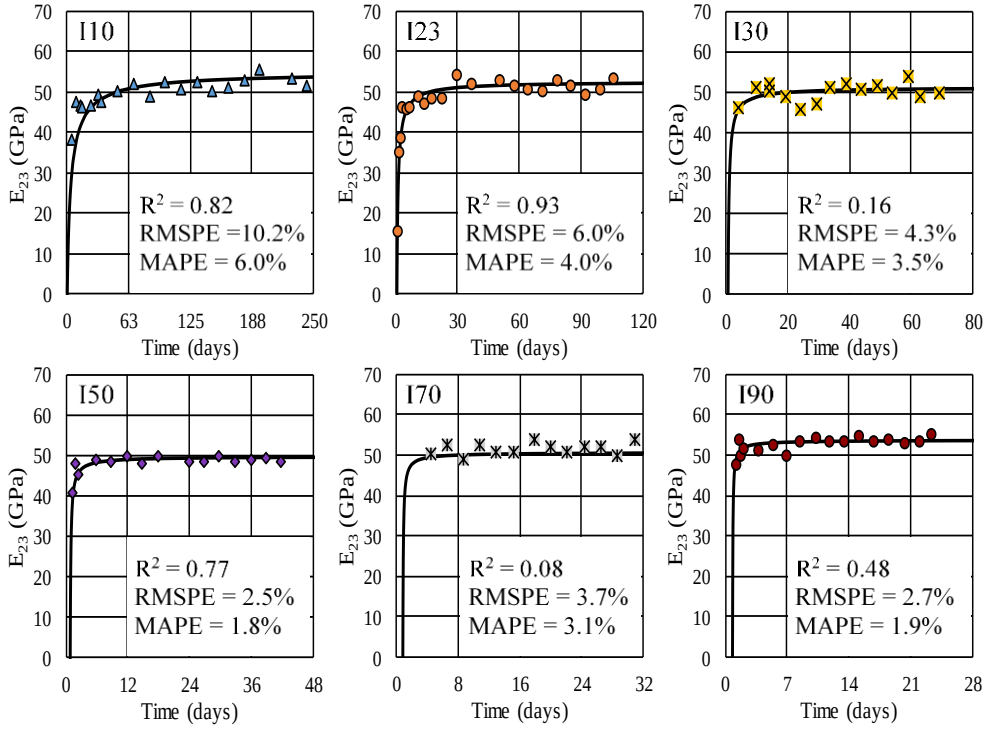

Figure 5.4 Elastic Modulus Measurements and Predictions

Figure 5.5 shows the relationship for f_c and E_{23} parametric functions versus dependent variables. Limit strength, f_{lim}, (Figure 5.5.a), limit elastic modulus, E_{lim}, (Figure 5.5.b), functions $a_f(T)$ and $a_E(T)$ (Figures 5.5.c and 5.5.d), and functions $b_f(T)$ and $b_E(T)$ (Figures 5.5.e and 5.5.f) are plotted against curing temperature. The rate functions, k_f (Figure 5.5.g) and k_E (Figure 5.5.h), are plotted for each curing temperature against time starting when time is greater than the offset value, t_0. Compressive strength and elastic modulus development trends at the six curing temperature are shown in Figures 5.5.i and 5.5.j, respectively. Curves between the 6 curing temperatures can be differentiated by location on Figures 5.5.g-j; higher values correspond to higher curing temperature. From Table 4.1, average and standard deviation of f_c values from 1900-2100°C-days are shown in Figure 5.5.a, most of which approach the limit strength trend line. As mentioned

previously, I50 strengths are lower than the expected linear trend. Average E_{23} values from Table 4.1 are shown in Figure 5.5.b. These values agree with the quadratic trend of E_{lim} with curing temperature and suggest that I50 curing yielded the lowest stiffness, similar to the results in Figure 4.2.

An advantage of this numerical formulation is that input values of time and temperature correspond to the state of the cured cylinders, simplifying physical interpretation of predictions and decision making. Considering applications of heat-treated UHPC, understanding the direct relationship between curing temperature and time can be very informative for construction decisions. In contrast, equivalent time methods require all abscissa to be transformed using a set of fit parameters. Final results of an equivalent time model need to be re-transformed back to the real age to understand real-time behavior. For construction related decisions – such as when to remove formwork – the output of these types of models could be miscommunicated, whereas all inputs and outputs of the proposed model are in basic units, making miscommunication less likely.

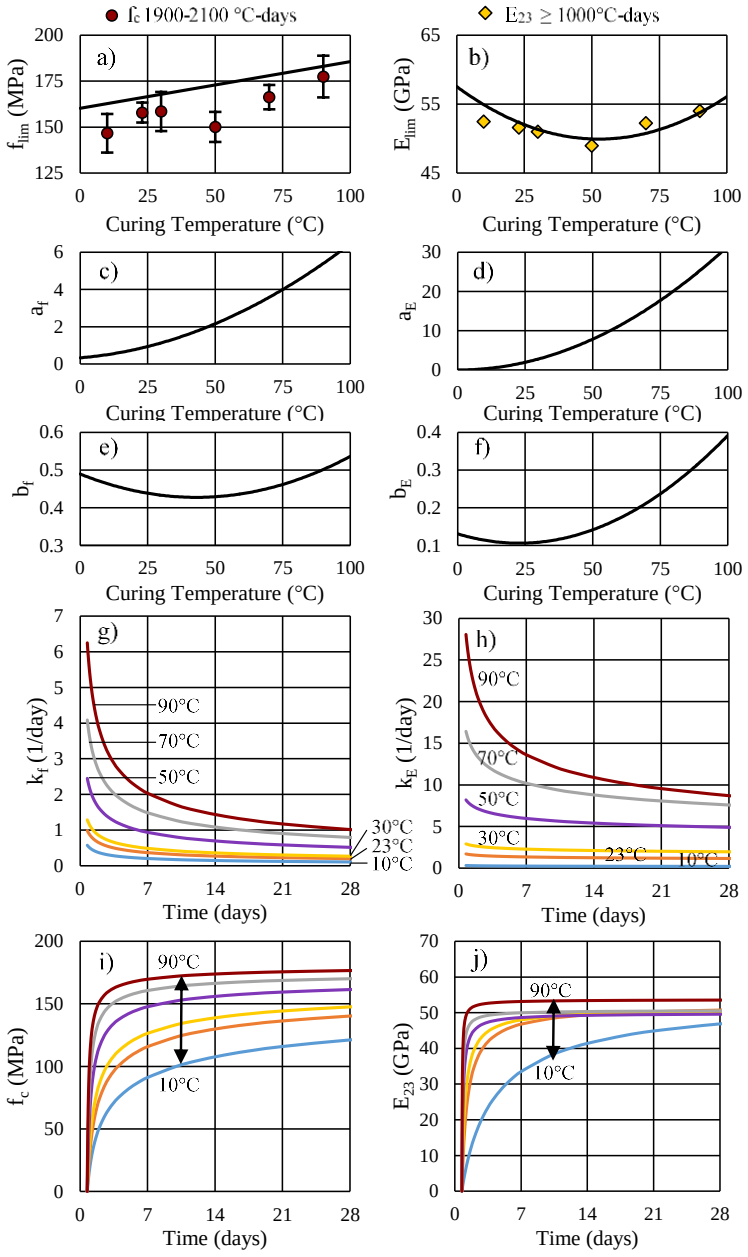

Figure 5.5 Parametric functions for selected Numerical Model

a.) f_{lim} vs. T, b.) E_{lim} vs. T, c.) a_f vs. T, d.) a_E vs. T, e.) b_f vs. T, f.) b_E vs. T, g.) k_f versus time for 6 temperatures, h.) k_E vs. time for 6 temperatures, i.) predicted f_c for isothermal curing groups, and j.) predicted E_{23} for isothermal curing groups.

CHAPTER VI

FINITE ELEMENT IMPLEMENTATION

This section describes the implementation of the selected numerical model in the Abaqus finite element analysis software. First, the parametric functions for compressive strength and elastic modulus are discretized. Then the discretized functions are written into a user defined field variable (USDFLD) subroutine to calculate and assign f_c and E_{23} values for the finite element model. For simplicity, the finite element model employs elasticity and perfectly plastic material description using E_{23} and f_c values, respectively, calculated by the subroutine. To verify that the formulation is valid, curing and C39 compression testing of cylindrical specimens are simulated in Abaqus and compared to experimental output.

6.1 Discretization of Numerical Model

A first order, two-dimensional Taylor series expansion is used to implement the model derived in Chapter V in a computational system. This approximate method requires differentiation with respect to both time and temperature. This two dimensional approximation is simplified by introducing numerical differentiation. A backwards difference scheme is used so that each differentiation is performed with previously calculated values. After derivation, the resulting formulae were coded into the USDFLD subroutine, which is not contained in this thesis.

The Taylor expansion for compressive strength predicts f_c for the next step, *i+1*, by considering the current f_c and the slope of f_c with respect to both time and temperature.

$$f_c(t + \Delta t_i, T + \Delta T_i) \approx f_c(t,T) + \frac{\partial}{\partial t} f_c(t,T)\Delta t_i + \frac{\partial}{\partial T} f_c(t,T)\Delta T_i \quad (6.1)$$

The general backwards difference form in Equation 6.2 can be used to approximate the time and temperature slopes between values at increments *i* and *i-1*. Taylor expansion uses steps Δt_i and ΔT_i while the backwards differentiation uses steps Δt_{i-1} and ΔT_{i-1}.

$$\frac{\partial}{\partial t} f(t) \approx \frac{f(t) - f(t - \Delta t_{i-1})}{\Delta t_{i-1}} \quad (6.2)$$

$$\Delta t_i = t_{i+1} - t_i,\ \Delta t_{i-1} = t_i - t_{i-1} \quad (6.3)$$

$$\Delta T_i = T_{i+1} - T_i,\ \Delta T_{i-1} = T_i - T_{i-1} \quad (6.4)$$

Substituting this form of differentiation into the Taylor expansion yields the following:

$$f_c(t + \Delta t_i, T + \Delta T_i) \approx f_c(t,T) + \frac{f_c(t,T) - f_c(t - \Delta t_{i-1}, T)}{\Delta t_{i-1}} \Delta t_i + \frac{f_c(t,T) - f_c(t, T - \Delta T_{i-1})}{\Delta T_{i-1}} \Delta T_i \quad (6.5)$$

Like terms can be collected and reduces to the following:

$$f_c(t + \Delta t_i, T + \Delta T_i) \approx$$

$$f_c(t,T)\left(1 + \frac{\Delta t_i}{\Delta t_{i-1}} + \frac{\Delta T_i}{\Delta T_{i-1}}\right) - f_c(t - \Delta t_{i-1}, T)\left(\frac{\Delta t_i}{\Delta t_{i-1}}\right) - f_c(t, T - \Delta T_{i-1})\left(\frac{\Delta T_i}{\Delta T_{i-1}}\right) \quad (6.6)$$

And can be represented in matrix form:

$$f_c(t + \Delta t, T + \Delta T) \approx$$

$$\begin{bmatrix} \left(1 + \frac{\Delta t_i}{\Delta t_{i-1}} + \frac{\Delta T_i}{\Delta T_{i-1}}\right) & -\left(\frac{\Delta t_i}{\Delta t_{i-1}}\right) & -\left(\frac{\Delta T_i}{\Delta T_{i-1}}\right) \end{bmatrix} \begin{bmatrix} f_c(t,T) \\ f_c(t - \Delta t_{i-1}, T) \\ f_c(t, T - \Delta T_{i-1}) \end{bmatrix} \quad (6.7)$$

For constant time and temperature steps, a much simpler formulation can be determined. Time step ratios cancel to equal 1 and the expansion reduces to the following:

$$f_c(t + \Delta t, T + \Delta T) \approx 3f_c(t,T) - f_c(t - \Delta t, T) - f_c(t, T - \Delta T) \quad (6.8)$$

And can be represented in matrix form:

$$f_c(t+\Delta t, T+\Delta T) \approx \begin{bmatrix} 3 & -1 & -1 \end{bmatrix} \begin{bmatrix} f_c(t,T) \\ f_c(t-\Delta t, T) \\ f_c(t, T-\Delta T) \end{bmatrix} \tag{6.9}$$

The same step discretization process is implemented for elastic modulus. As discussed in the next section, time incrementation in Abaqus is automatically adjusted, so time steps are not necessarily equal. Therefore, the matrix form in Equation 6.7 is used. These formulas were coded into a user defined field variable (USDFLD) subroutine in FORTRAN.

When implemented, Equation 6.7 (and 6.9) predicts f_c and E_{23} for the next time increment by calculating the three terms in the column matrix on the right hand side. As temperature changes and time marches forward, equation 6.7 interpolates between time and temperature by combining three weighted predictions. Because this model simply interpolates, predictions are limited to fall on or within the isothermal curves seen in Figures 5.5.i and 5.5.j. For this reason, the accuracy of predictions for temperatures above 90°C or below 10°C are unknown. To capture non-isothermal temperature effects on strength at early ages or delayed heat treatment (e.g. curing of M specimens), modifications are needed.

6.2 Finite Element Model Description

Twenty four simulations were performed, corresponding to 6 curing temperatures (10, 23, 30, 50, 70, and 90°C) and 4 durations (1, 7, 14, and 28 days) to test the implementation of the isothermal strength development model. All cylinder models had the same geometry with a diameter of 4 inches (0.102 m) and height of 8 inches (0.203 m). A relatively coarse mesh of 320 elements and was used, which helped reduce calculation

time. Element type is C3D8T which corresponds to 8 noded, linear continuum brick elements which are formulated for coupled thermal-stress analyses. This mesh was deemed suitable for testing the implementation of the numerical model. Figure 6.1 shows the meshed geometry.

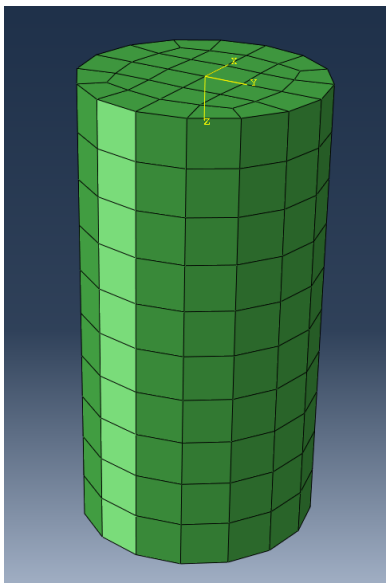

Figure 6.1 Meshed Cylinder Geometry

Curing was simulated for the six curing temperatures by setting thermal boundary conditions on the surface of the cylinder equal to the curing temperature. The curing temperature boundary condition was allowed to change with time by applying a ramp profile. A ramp profile allowed the curing temperature to begin at 23°C, stay at 23°C for 24 hours, and then ramp to the target temperature over 6 hours. Curing was divided into two steps to provide more resolution at early ages when the most strength gain occurs. All units of the simulations were in the “SI kg-m” system.

After the two curing steps, compression testing according to ASTM C39 was simulated. The bottom of the cylinder was fixed from displacement, but allowed to expand diametrically. This prevented the development of confinement stresses which can occur if all points on the bottom surface are fully fixed. Loading was applied by displacing the top surface of the cylinder at a rate of $1.0*10^{-6}$ m/s. This displacement induces a uniform, uniaxial stress state. The selected loading rate corresponds to the ASTM C39 stress rate of 0.24 MPa/s (35 psi/s) for a cylinder with a stiffness of 49 GPa. Most cylinders achieved at least this stiffness, however, specimens tested at 1 day ended up being strained at a rate far below the requirements of ASTM C39. Nonetheless, for the goals of these simulations, this loading configuration was deemed suitable. Table 6.1 shows the incrementation details for each of the three simulation steps.

Table 6.1 Incrementation Details for each Step

Parameter	**Cure Step 1**	**Cure Step 2**	**C39 Loading**
Duration	7200 sec.	Age[sec.] – 7200 sec.	1800 sec.
Initial Δt	1 sec.	30 sec.	3 sec.
Min. Δt	1 sec.	30 sec.	0.05 sec.
Max. Δt	60 sec.	7200 sec.	60 sec.
Max. number of increments	3600	3600	1000

Input files were modified to work with the USDFLD subroutine. Six dependent variables are passed through USDFLD for each time step. Two variables are E and f_c, while the other four keep track of temperature, time, time increments, and temperature increments. The GETVRM utility subroutine passes material point information into the USDFLD routine and was used to access temperature data. The material properties for E and f_c are assigned to elastic modulus and the perfectly plastic yield limit at each integration

point as each time increment is calculated. These materials properties were very unrealistic for representing behavior of this material, but allowed for easy sampling of the developed mechanical property data. The only other mechanical property defined was the Poisson ratio which was selected to be 0.15. Thermal properties were input with specific heat of 960 J/kg-K and thermal conductivity of 2.0 W/m-K. A density of 2520 kg/m^3 was input.

6.3 Finite Element Model Results

The maximum principal stress was seen to be constant, indicating the uniaxial stress state was achieved. Figure 6.3 shows the stress vs. strain output from the loading step of the simulations. These plots clearly show that the slope of the loading curve is constant, corresponding to the elastic modulus, until the "yield limit" is reached, which corresponds to the compressive strength.

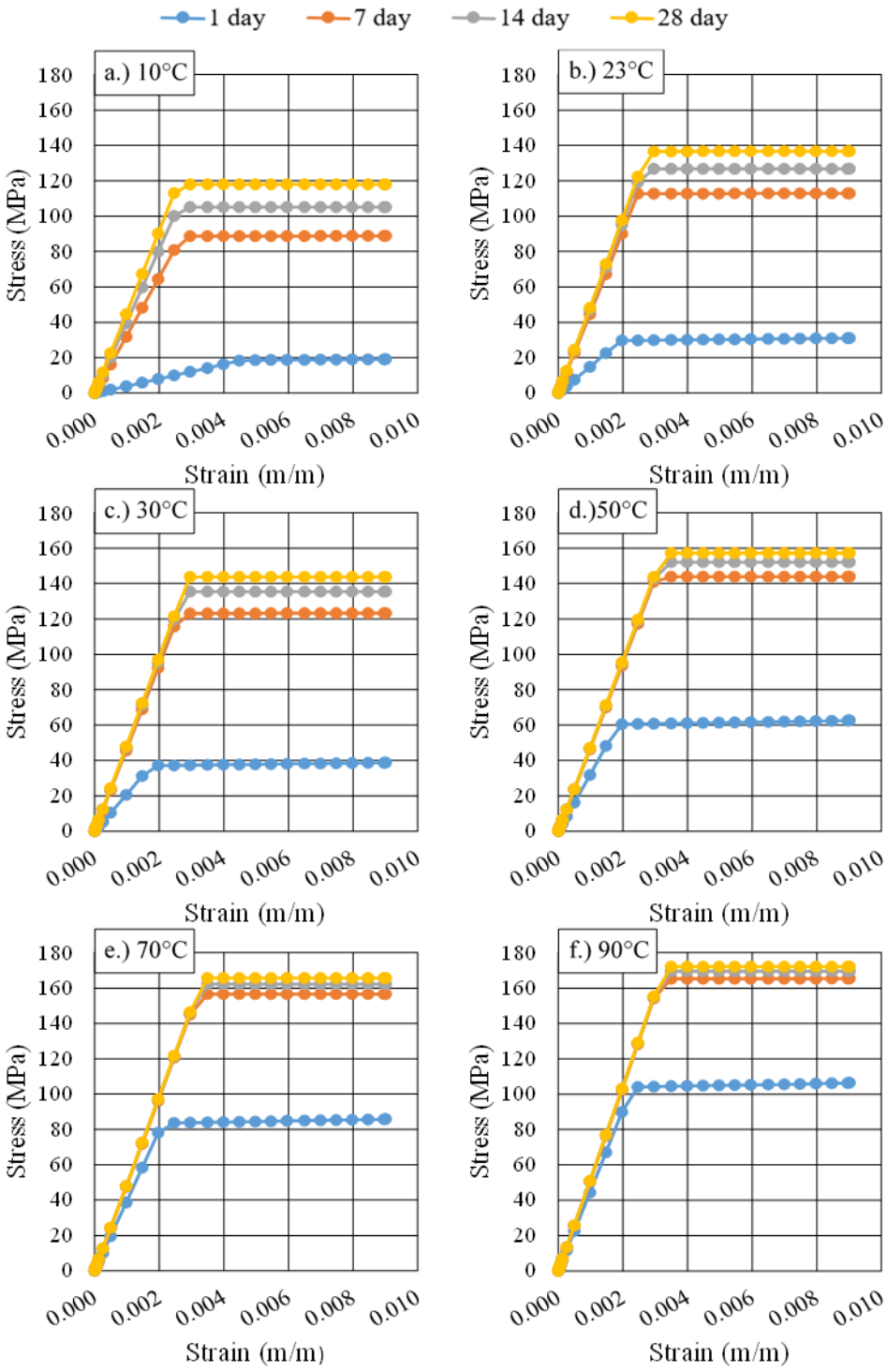

Figure 6.2 Results of C39 Uniaxial Compression Test in Abaqus

Tables 6.2 and 6.3 summarize the resulting E and f_c values achieved through the curing simulation and sampled from data contained in Figure 6.2. The resulting values calculated by Abaqus are compared to model predictions (equations in table 5.2) assuming a constant curing temperature. All differences for f_c are within 5 MPa and for E are within 1.6 GPa. All of these errors correspond to less than a 5% difference. The discrepancies between these simulations and predictions are small, but may be due to the curing simulation which changes temperature over the first 30 simulation hours. Overall, the goal of this study was achieved and the numerical model was successfully implemented.

Table 6.2 Compressive strength: FEA vs. calculated with model parameters

Curing	Compressive Strength (MPa)			
Temp.	1d	7d	14d	28d
10	19.2 (-0.8)	88.8 (2.3)	105.1 (2.5)	118.0 (3.1)
23	31.1 (-1.1)	112.8 (2.9)	126.7 (3.2)	136.6 (3.7)
30	38.8 (-1.2)	123.2 (3.2)	135.4 (3.4)	143.8 (3.8)
50	62.7 (-1.3)	143.9 (3.8)	152.1 (3.9)	157.3 (4.1)
70	85.9 (-1.0)	156.6 (4.1)	162.2 (4.2)	165.7 (4.4)
90	106.4 (-0.5)	165.3 (4.4)	169.5 (4.4)	172.1 (4.5)

--Values in parentheses are (predicted f_c – FEA $f_{c)}$

Table 6.3 Elastic modulus: FEA vs. calculated with model parameters

Curing	Elastic Modulus (GPa)			
Temp.	1d	7d	14d	28d
10	4.0 (0.1)	32.7 (0.8)	40.5 (0.9)	45.7 (1.2)
23	15.2 (0.3)	45.7 (1.1)	48.3 (1.1)	49.6 (1.2)
30	21.0 (0.5)	46.8 (1.2)	48.3 (1.3)	49.1 (1.3)
50	32.3 (1.0)	47.4 (1.3)	48.0 (1.3)	48.3 (1.3)
70	39.4 (1.1)	48.7 (1.3)	49.1 (1.2)	49.2 (1.3)
90	45.3 (1.3)	51.6 (1.6)	52.1 (1.3)	52.2 (1.4)

--Values in parentheses are (predicted E – FEA E)

CHAPTER VII

CONCLUSIONS

An experimental dataset was generated for Cor-Tuf UHPC to demonstrate the time- and temperature-dependent nature of mechanical properties, specifically compressive strength and elastic modulus. The extent and rate of f_c development in Cor-Tuf UHPC is shown to be heavily influenced by the curing temperature. Higher temperature curing also showed the highest variability and visual scatter. The rate of E development increased with curing temperature, while the overall extent was limited to a range between 49 and 54 GPa that did not follow a linear trend with curing temperature. Elastic modulus at the time of testing is shown to depend heavily on specimen temperature and an equation is proposed to adjust results to an equivalent room temperature measurement. Mixed temperature curing appears to develop similar or higher strengths than I90 specimens at the same age or maturity, despite following a delay to high temperatures exposure for shorter durations. These mixed temperature results suggests that delaying heat exposure may benefit development of strength.

Numerically predicted strength and modulus for category I specimens agrees well with measured values with an average R^2 of 0.68, RMSPE of 8.3%, and MAPE of 5.8% for f_c and an average R^2 of 0.58, RMSPE of 5.2%, and MAPE of 3.5% for E_{23}. A quadratic trend is predicted for the limiting E that agrees well with averaged data after maturities of

1000°C-days. The numerical model was discretized and successfully implemented in Abaqus finite element software.

An advantage of this numerical formulation is that input values of time and temperature correspond to the state of the cured cylinders in real-time, simplifying physical interpretation of predictions. Considering applications of heat-treatment and mass concrete, understanding the direct relationship between curing temperature and time is informative for construction decisions (such as formwork type and time of removal) to balance performance and cost of UHPC. Numerical modeling efforts should be extended from isothermal conditions to variable temperature profiles of laboratory cylinders and subsequently full-scale structures for a variety of UHPC mixtures and properties (e.g. tensile strength).

A numerical framework is under development by MSU which strives to recursively simulate and optimize the material selection, construction, and behavior of UHPC structures supplemented with directly measured mechanical properties. Work by Fairbairn et al. (2004) showcases the capability of a similar framework applied for conventional concrete to minimize cost without sacrificing performance or constructability. Paired with a heat development model, a full-scale structural simulation could use a material development scheme to optimize construction parameters for a given UHPC mixture. The proposed models provide a method to extend predictive capabilities to UHPC mixtures and a step toward realizing the current MSU research goals.

REFERENCES

ACI 209R-13, "Prediction of Creep, Shrinkage, and Temperature Effects in Concrete Structures," *ACI Manual of Concrete Practice,* Part 1, American Concrete Institute, Farmington Hills, Michigan, 2013.

ACI 318R-11, "Building Code Requirements for Structural Concrete," *ACI Manual of Concrete Practice,* Part 3, American Concrete Institute, Farmington Hills, Michigan, 2013.

ACI 363R-13, "Report on High-Strength Concrete," *ACI Manual of Concrete Practice,* Part 5, American Concrete Institute, Farmington Hills, Michigan, 2013.

ASTM C1074-17, "Standard Practice for Estimating Concrete Strength by the Maturity Method," ASTM International, West Conshohocken, PA.

Ahmad, S.; and Hakeem, I., "Effect of curing, fibre content and exposures on compressive strength and elasticity of UHPC," *Advances in Cement Research,* Vol. 27, No. 4, 2015, pp. 233-239.

Alsalman, A.; Dang, C.N.; Prinz, G.S.; and Hale, W.M., "Evaluation of Modulus of Elasticity of Ultra-High Performance Concrete," *Construction and Building Materials,* Vol. 153, 2017, pp. 918-928.

Andersen, L. W.; Ruzzante, D. E.; Walton, M.; Berggren, P.; Bjorge, A.; and Lockyer, C., "Nonlinear, Incremental Structural Analysis of Massive Concrete Structures." U.S. Army Corps of Engineers, Technical Letter No. 1110-2-365, 1994, pp.1-76.

Berry, M; Snidarich, R.; and Wood, C., "Development of Non-Proprietary Ultra-High Performance Concrete," Report FHWA/MT-17-010/8237-001 Bozeman, MT, December 2017.

Carino, N.J., "The Maturity Method: Theory and Application," *Cement, Concrete, and Aggregates* Vol. 6, No. 2, winter 1984, pp. 61-73.

Carino, N.J.; and Lew, H.S., "The Maturity Method: From Theory to Application," *Proceedings of the 2001 Structures Congress & Exposition, American Society of Civil Engineers.* Reston, Virginia. May 2001.

Cervera, M.; Faria, R.; Oliver, J.; and Prato, T., "Numerical Modelling of Concrete Curing, Regarding Hydration and Temperature Phenomena," *Computers and Structures* Vol. 80, 2002, pp. 1511-1521.

Cervera, M.; Oliver, J.; and Prato, T., "Thermo-Chemo-Mechanical Model for Concrete. I: Hydration and Aging," *Journal of Engineering Mechanics* Vol. 125, No. 9, 1999, pp. 1018-1027.

D'Aloia, L.; and Chanvillard, G., "Determining the "Apparent" Activation Energy of Concrete E_a – Numerical Simulations of the Heat of Hydration of Cement," *Cement and Concrete Research* Vol. 32, 2002, pp. 1277-1289.

Di Luzio, G.; and Cusatis, G., "Hygro-Thermo-Chemical Modeling of High Performance Concrete. I: Theory," *Cement & Concrete Composites* Vol. 31, 2009, pp. 301-308.

Fairbairn, E.; Silvoso, M.; Toledo Filho, R.; Alves, J.; and Ebecken, N., "Optimization of Mass Concrete Construction using Genetic Algorithms," *Computers & Structures* Vol. 82, 2004, pp. 281-299.

Faria, R.; Azenha, M.; and Figueiras, J.A., "Modelling of Concrete at Early Ages: Application to an Externally Restrained Slab," *Cement & Concrete Composites* Vol. 28, 2006, pp. 572-585.

Gajda, J., "Mass Concrete for Buildings and Bridges," *Portland Cement Association,* EB547 Skokie, Illinois, 2007.

Graybeal, B., "Material Property Characterization of Ultra-High Performance Concrete," Report FHWA-HRT-06-103 McLean, VA, August 2006.

Graybeal, B., "Ultra-High Performance Concrete," Technical Note FHWA-HRT-11-083 McLean, VA, 2011.

Green, B.H.; Moser, R.D.; Scott, D.A.; and Long, W.R., "Ultra-High Performance Concrete History and Usage by the Corps of Engineers," *Advances in Civil Engineering Materials*, Vol. 4, No. 2, 2015, pp. 132-143.

Habel, K.; Viviani, M.; Denarié, E.; and Brühwiler, E., "Development of the Mechanical Properties of an Ultra-High Performance Fiber Reinforced Concrete (UHPFRC)," *Cement and Concrete Research* Vol. 36, 2006, pp. 1362-1370.

Howard, I.; Carey, A.; Burcham, M.; Scott, D.; Moser, R.; and Horsetmeyer, M., "Constituent Properties of Cor-Tuf Ultra-High-Performance Concrete," Report Currently in Sponsor Review, 2018a.

Howard, I., Allard, T, Carey, A., Priddy, M., Knizley, A., Shannon, J., "Development of CORPS-STIF 1.0 with Application to Ultra-High Performance Concrete (UHPC)," Draft Report in Development, 2018b.

Kim, J.K.; Han, S.H.; and Lee, K.M., "Estimation of Compressive Strength by a New Apparent Activation Energy Function," *Cement and Concrete Research* Vol. 31, 2001, pp. 217-225.

Kim, J.-K.; Moon, Y.-H.; and Eo, S.-H., "Compressive Strength Development of Concrete with Different Curing Time and Temperature," *Cement and Concrete Research* Vol. 28, No. 12, 1998, pp. 1761-1773.

Korpa, A.; and Trettin, R., "Very high early strength of ultra-high performance concrete containing nanoscale pozzolans using the microwave heat curing method," *Advances in Cement Research* Vol. 20, No. 4, 2008, pp. 175-184.

Lee, C.; Lee, S.; and Nguyen, N., "Modeling of Compressive Strength Development of High-Early-Strength-Concrete at Different Curing Temperatures," *International Journal of Concrete Structures and Materials* Vol. 10, No. 2, June 2016, pp. 205-219.

Liu, Z.; Chen, W.; Zhang, W.; Zhang, Y.; and Lv, H., "Complete Stress-Strain Behavior of Ecological Ultra-High Performance Composite under Uniaxial Compression," *ACI Materials Journal* Vol. 114, No. 5, 2017, pp. 783-794.

Logan, S. R., "The Origin and Status of the Arrhenius Equation," *Journal of Chemical Education* Vol. 59, No. 4, April 1982, pp. 279-281.

Maage, M., "Strength and Heat Development in Concrete: Influence of Fly Ash and Condensed Silica Fume," ACI Special Publication 91, 1986 pp. 923-940.

Oliphant, T. E., "Python for Scientific Computing," *Computing in Science & Engineering* Vol. 9, No. 3, 2007, pp. 10-20.

Prem, P. R.; Murthy, A. R.; and Bharatkumar, B. H., "Influence of curing regime and steel fibres on the mechanical properties of UHPC," *Magazine of Concrete Research* Vol. 67, No. 18, 2015, pp. 988-1002.

Rossum, G. V., "Python Tutorial," Technical Report CS-R9526, Centrum voor Wiskunde en Informatica (CWI), Amsterdam, May 1995.

Sbia, L.A.; Peyvandi, A.; Harsini, I.; Lu, J.; Abideen, S.U.; Weerasiri, R.R.; Balachandra, A.M.; and Soroushian, P., "Study on Field Thermal Curing of Ultra-High Performance Concrete Employing Heat of Hydration," *ACI Materials Journal* Vol. 114, No. 5, October 2017, pp. 733-744.

Shah, S. P.; and Konsta-Gdoutos, M. S., "Uncoupling Modulus of Elasticity and Strength," *Concrete International* Vol. 39, No. 11, 2017, pp. 37-42.

Ulm, F.; and Coussy, O., "Modeling of Thermochemomechanical Couplings of Concrete at Early Ages," *Journal of Engineering Mechanics* Vol. 121, No. 7, July 1995, pp. 785-794.

Wan, L.; Wendner, R.; Liang, B.; and Cusatis, G., "Analysis of the Behavior of Ultra High Performance Concrete at Early Age," *Cement & Concrete Composites* Vol. 74, 2016, pp. 120-135.

Williams, E.; Graham, S.; Reed, P.; and Rushing, T., "Laboratory Characterization of Cor-Tuf Concrete With and Without Steel Fibers," ERDC/GSL TR-09-22.

APPENDIX A

RAW EXPERIMENTAL DATA FOR ISOTHERMAL CURING GROUP

A.1 Mechanical Testing Results of Isothermal Curing

Table A.1 Mechanical Testing Results of I10 Cylinders

Age (days)	Maturity (°C-days)	f_c (MPa)	E (GPa)	Density (g/cm^3)	Age (days)	Maturity (°C-days)	f_c (MPa)	E (GPa)	Density (g/cm^3)
4.0	53.8	78.4	---	2.496	115.0	1165.5	140.5	52.0	2.549
4.0	53.8	79.2	39.4	2.514	118.9	1204.4	150.6	---	2.551
5.0	62.6	87.3	---	2.513	123.5	1249.3	126.3	---	---
5.0	63.2	84.8	---	2.504	126.8	1281.8	139.6	---	2.566
7.2	84.4	90.6	---	---	131.0	1323.9	151.4	53.7	2.527
9.3	104.4	99.3	---	2.527	134.5	1359.1	146.7	---	2.541
9.3	104.8	95.7	48.6	2.525	139.2	1409.6	132.1	---	2.541
11.1	122.3	98.0	---	2.529	142.5	1454.1	139.8	---	2.541
13.0	141.3	99.2	---	2.526	147.0	1506.9	138.0	51.5	2.530
13.1	141.0	101.8	48.0	2.532	151.0	1553.9	142.1	---	2.562
15.4	165.8	108.5	47.3	2.517	155.0	1601.3	148.9	---	2.517
19.3	204.3	111.5	---	2.522	159.0	1648.1	156.8	---	2.537
23.3	243.2	103.4	47.8	2.533	163.0	1696.2	143.1	52.2	2.544
27.2	281.7	118.8	---	2.514	167.0	1742.6	141.0	---	2.547
31.1	320.0	114.9	50.4	2.511	170.9	1789.2	137.3	---	2.526
34.9	377.2	126.8	48.7	---	175.0	1792.2	141.2	---	2.546
38.6	414.4	118.1	---	---	179.0	1831.0	142.9	53.9	2.535
42.9	456.8	123.3	---	---	183.0	1869.6	147.4	---	2.541
47.0	497.3	111.2	---	---	187.0	1908.4	151.6	---	2.548
50.8	534.5	131.1	51.5	---	190.9	1946.6	144.7	---	2.550
55.0	575.6	137.9	---	2.522	195.1	1987.1	140.0	56.9	2.551
58.9	614.5	142.8	---	2.562	199.0	2025.0	145.2	---	2.559
62.9	653.8	135.6	---	2.540	203.0	2064.0	151.7	---	2.549
67.0	693.9	131.0	53.0	2.517	207.3	2106.0	159.8	---	2.556
70.9	732.3	133.8	---	2.566	211.0	2142.4	146.4	---	2.527
75.1	773.5	137.2	---	2.537	214.8	2188.6	160.7	---	2.541
78.9	810.7	151.2	---	2.567	219.1	2232.5	145.2	---	2.526
82.9	850.1	140.8	49.9	2.547	222.8	2269.8	155.4	---	2.544
87.0	890.7	129.7	---	2.539	226.9	2311.9	146.2	54.5	2.532
90.9	928.5	144.4	---	2.534	231.0	2353.9	156.2	---	2.536
94.9	968.0	141.7	---	2.529	235.0	2394.0	142.8	---	2.532
98.9	1007.7	135.3	53.8	2.538	238.9	2433.1	118.8	---	---
103.0	1047.8	139.2	---	2.516	243.0	2476.1	153.7	52.7	2.530
107.1	1088.4	151.7	---	2.560	248.8	2534.2	153.9	---	2.546
111.1	1127.0	137.0	---	2.543	251.0	2557.1	151.6	---	2.558

Table A.2 Mechanical Testing Results of I23 Cylinders

Age (days)	Maturity (°C-days)	f_c (MPa)	E (GPa)	Density (g/cm^3)	Age (days)	Maturity (°C-days)	f_c (MPa)	E (GPa)	Density (g/cm^3)
0.7	16.1	2.9	---	---	47.0	986.5	156.0	---	2.542
0.7	16.2	2.7	---	---	48.8	1022.9	145.6	---	2.509
1.0	21.5	17.1	---	---	50.6	1060.7	148.8	52.8	---
1.0	21.7	20.6	15.4	---	52.3	1095.8	146.5	---	2.509
1.5	32.3	55.8	---	---	54.0	1132.2	167.1	---	2.528
1.5	32.5	61.0	35.1	---	55.7	1168.4	155.5	---	2.534
2.0	43.1	75.7	---	---	57.6	1206.4	160.3	51.7	2.519
2.0	43.4	76.4	38.8	---	59.3	1242.3	166.6	---	---
2.5	53.9	90.4	---	---	61.1	1280.2	159.5	---	2.505
3.0	63.2	92.0	---	---	62.7	1313.9	162.3	---	---
3.0	63.4	99.5	46.4	---	64.4	1348.9	149.3	51.0	2.518
3.5	74.5	97.7	---	---	66.3	1389.6	153.4	---	2.551
4.0	84.8	103.7	---	---	68.0	1424.5	148.0	---	2.491
5.0	105.7	100.6	---	---	69.6	1459.5	150.5	---	2.538
5.0	105.8	110.4	45.9	---	71.3	1494.8	130.1	50.2	---
6.0	126.7	114.1	---	---	73.1	1532.6	150.1	---	2.539
7.0	147.2	112.1	46.2	2.517	75.0	1571.2	150.0	---	2.525
8.8	185.4	120.7	---	2.535	76.5	1603.7	162.7	---	2.552
10.7	224.0	117.6	49.0	2.536	78.9	1654.2	147.8	52.9	2.523
12.2	257.0	116.8	---	2.498	80.5	1687.8	140.5	---	2.523
14.0	293.2	121.6	47.3	2.507	81.9	1716.6	160.0	---	2.543
15.9	334.0	117.5	---	---	83.5	1749.5	157.2	---	2.525
17.4	364.7	132.4	48.7	---	85.2	1785.8	163.3	51.7	2.533
19.2	404.4	126.1	---	---	87.0	1823.4	155.3	---	2.542
20.9	439.8	129.9	---	---	88.9	1863.0	149.4	---	2.514
22.8	478.7	134.1	48.4	---	90.4	1895.0	164.3	---	2.542
24.5	513.5	138.8	---	---	92.3	1932.9	152.7	49.6	2.514
26.2	549.7	135.2	---	---	93.9	1968.3	164.2	---	2.557
28.0	586.8	148.6	---	---	95.8	2008.2	143.4	---	2.536
29.7	622.3	139.4	54.2	---	97.4	2041.3	148.5	---	2.508
31.4	658.0	144.3	---	2.503	99.2	2077.5	152.4	51.0	2.539
33.2	696.1	140.3	---	2.515	101.0	2115.7	161.5	---	2.532
34.9	732.3	111.2	---	2.520	102.8	2153.4	155.0	---	2.544
36.7	769.5	156.9	51.9	---	104.8	2197.0	148.0	---	2.538
38.3	802.9	140.3	---	---	106.2	2224.4	158.4	53.6	2.532
40.1	840.7	126.7	---	---	107.9	2261.1	148.0	---	2.526
41.8	876.9	141.2	---	---	109.7	2299.2	155.9	---	2.527
43.7	915.2	151.5	62.7	---	111.3	2331.9	155.3	---	2.530
45.3	949.3	152.3	---	2.530					

Table A.3 Mechanical Testing Results of I23M Cylinders

Age (days)	Maturity (°C-days)	f_c (MPa)	E (GPa)	Density (g/cm^3)	Age (days)	Maturity (°C-days)	f_c (MPa)	E (GPa)	Density (g/cm^3)
0.8	16.5	3.1	---	2.493	45.4	1041.7	136.7	47.4	2.520
0.8	16.5	3.4	---	2.488	47.1	1082.1	131.8	---	2.517
1.0	20.3	17.0	---	2.505	48.8	1120.3	124.6	---	2.492
1.0	21.3	7.5	---	---	50.5	1160.5	132.8	---	2.524
1.1	24.0	23.5	14.5	---	52.2	1199.2	130.6	46.5	2.506
1.1	24.2	33.1	---	---	54.0	1241.3	133.9	---	2.506
1.2	26.6	33.5	---	---	55.7	1280.0	135.8	---	2.494
1.5	33.3	53.3	---	2.514	57.4	1318.5	145.9	---	2.535
1.5	33.3	56.9	33.9	2.502	59.2	1360.6	139.9	48.2	2.520
1.5	32.1	55.4	---	---	61.0	1402.2	140.1	---	2.509
1.7	36.2	66.2	---	---	62.8	1443.7	143.7	---	2.516
2.1	44.5	69.3	---	---	64.4	1479.3	136.0	---	2.519
3.0	67.6	82.1	---	---	66.2	1521.1	134.7	46.5	2.536
4.0	90.2	88.6	---	---	68.0	1561.9	133.6	---	2.519
5.1	114.3	90.9	---	---	69.7	1600.2	127.5	---	2.519
6.1	137.3	94.1	---	---	71.3	1638.6	127.2	---	2.514
7.0	159.2	93.9	---	---	73.2	1681.2	137.0	45.4	2.522
8.9	203.6	104.2	---	---	75.0	1722.4	140.3	---	2.517
10.6	241.0	118.0	43.1	---	76.5	1758.3	140.8	---	2.522
12.3	280.8	119.2	---	---	78.3	1799.2	134.1	---	2.523
14.0	320.9	118.9	---	---	80.0	1838.4	144.3	49.1	2.527
15.8	362.0	117.0	---	---	81.8	1880.6	136.7	---	2.526
17.5	399.3	125.1	45.8	---	83.5	1918.4	143.4	---	2.497
19.3	442.5	122.0	---	---	85.3	1961.2	138.6	---	2.508
21.0	480.7	128.9	---	---	87.1	2000.7	137.2	47.4	2.538
22.8	523.2	124.0	---	---	88.8	2040.8	130.7	---	2.529
24.5	562.3	128.4	46.2	---	90.5	2079.0	135.2	---	2.486
26.3	602.4	112.5	---	2.518	92.2	2120.2	131.7	---	2.509
27.9	640.3	120.7	---	---	94.1	2161.7	125.1	43.5	2.523
29.8	683.2	140.0	---	---	95.7	2200.1	135.7	---	2.522
31.3	719.0	134.1	47.1	---	97.4	2238.4	135.3	---	2.512
33.2	761.0	126.0	---	---	99.2	2279.9	137.5	---	2.512
34.9	800.7	107.5	---	---	101.0	2321.4	138.8	45.0	2.516
36.7	840.7	131.7	---	---	102.8	2362.0	148.8	---	2.528
38.3	879.2	131.7	45.8	---	104.3	2398.5	130.9	---	2.510
40.1	920.9	133.6	---	---	106.2	2429.8	134.1	---	2.513
41.8	960.6	131.7	---	2.503	108.0	2482.1	138.0	45.6	2.519
43.5	998.2	137.5	---	2.518	109.7	2522.2	149.1	---	---

Table A.4 Mechanical Testing Results of I30 Cylinders

Age (days)	Maturity (°C-days)	f_c (MPa)	E (GPa)	Density (g/cm^3)	Age (days)	Maturity (°C-days)	f_c (MPa)	E (GPa)	Density (g/cm^3)
3.7	99.2	101.5	45.8	---	38.8	1152.7	146.4	51.6	---
5.3	148.7	117.5	---	2.517	40.4	1200.6	145.3	---	2.517
7.0	199.3	137.1	---	2.538	42.0	1248.5	129.2	---	2.508
9.6	278.3	140.4	50.8	2.521	43.7	1300.5	164.1	50.1	---
10.3	300.4	140.0	---	2.503	45.3	1349.4	156.4	---	2.509
12.0	350.0	147.8	---	2.534	47.0	1398.7	166.8	---	2.527
13.7	401.4	136.4	51.6	2.516	48.6	1448.5	165.4	51.0	---
13.7	401.6	71.9	49.8	2.531	50.3	1498.7	135.7	---	2.519
15.4	452.0	160.1	---	2.536	52.1	1553.0	154.9	---	2.529
17.2	497.8	139.2	---	2.500	53.8	1603.1	160.4	49.2	2.529
18.9	548.4	146.7	48.6	---	55.3	1649.3	161.4	---	2.529
20.6	600.3	145.6	---	2.517	57.1	1702.0	162.6	---	2.505
22.2	647.8	134.8	---	2.490	58.8	1753.1	162.4	53.2	2.528
23.9	699.8	133.6	45.2	2.502	60.4	1802.3	160.0	---	2.507
25.6	750.6	139.6	---	2.520	62.0	1851.6	140.8	---	2.527
27.3	801.3	130.8	---	2.509	62.8	1872.9	147.9	48.4	2.546
28.9	851.1	150.1	46.6	2.517	65.4	1953.9	162.8	---	2.516
30.4	900.1	161.6	---	2.534	67.0	2000.3	160.6	---	2.526
32.0	950.5	152.2	---	2.514	68.7	2052.8	161.9	49.3	2.509
33.7	999.7	159.4	50.7	---	70.3	2098.1	148.7	---	2.534
35.3	1048.7	150.8	---	2.532	72.0	2150.5	164.0	---	2.527
37.0	1099.8	156.0	---	2.525					

Table A.5 Mechanical Testing Results of I50 Cylinders

Age (days)	Maturity (°C-days)	f_c (MPa)	E (GPa)	Density (g/cm^3)	Age (days)	Maturity (°C-days)	f_c (MPa)	E (GPa)	Density (g/cm^3)
1.3	37.5	87.9	---	2.495	19.9	949.8	148.7	---	2.516
1.3	37.8	86.9	38.9	2.514	21.0	1002.1	146.4	---	2.517
1.6	49.9	106.0	---	2.482	21.9	1048.5	138.8	---	2.526
1.9	65.0	126.1	46.0	2.524	22.9	1098.3	157.2	---	2.521
1.9	65.1	118.7	---	2.501	23.9	1147.6	161.1	46.5	2.504
2.0	73.1	130.0	---	2.541	24.9	1200.6	156.7	---	2.522
2.2	85.4	119.0	---	2.506	25.9	1248.6	151.1	---	2.533
2.3	85.4	126.7	43.3	2.492	26.9	1298.9	139.3	46.2	2.502
2.9	99.0	129.6	---	---	27.9	1350.1	154.0	---	2.530
3.9	148.8	133.1	---	---	28.8	1397.6	139.3	---	---
4.9	199.1	135.6	---	---	29.8	1446.3	165.1	47.7	2.518
5.9	248.9	145.7	46.6	---	30.9	1499.2	157.6	---	2.510
6.9	299.0	146.9	---	---	31.9	1548.0	152.0	---	2.515
7.9	348.7	146.1	---	---	32.9	1597.5	150.2	46.5	2.503
8.8	397.5	154.1	46.4	---	33.9	1648.8	127.9	---	2.532
9.8	448.1	149.3	---	---	35.0	1701.4	148.1	---	2.511
10.9	499.4	148.2	---	---	35.9	1748.3	152.7	46.8	2.503
11.9	549.3	165.3	47.8	---	36.9	1797.7	147.8	---	2.515
12.8	598.3	149.6	---	2.501	37.9	1848.2	154.8	---	2.527
13.8	647.5	138.2	---	2.485	39.0	1900.4	155.1	47.4	2.529
14.8	698.1	161.8	45.9	---	39.9	1948.0	145.6	---	2.496
15.9	749.7	149.1	---	2.510	40.9	1999.5	155.1	---	2.510
17.0	800.0	165.5	---	2.535	41.9	2048.0	151.8	46.5	2.511
17.9	848.0	167.3	47.8	2.514	42.9	2097.6	142.6	---	2.526
18.9	897.4	159.9	---	2.489	43.9	2147.8	159.7	---	2.512

Table A.6 Mechanical Testing Results of I70 Cylinders

Age (days)	Maturity (°C-days)	f_c (MPa)	E (GPa)	Density (g/cm^3)	Age (days)	Maturity (°C-days)	f_c (MPa)	E (GPa)	Density (g/cm^3)
2.2	98.2	144.6	---	---	17.7	1147.0	159.3	50.2	2.514
3.0	150.2	152.0	---	---	18.4	1195.4	171.6	---	2.527
3.6	197.8	166.0	---	---	19.1	1245.3	166.3	---	2.523
4.3	246.6	169.1	46.7	---	19.8	1296.8	174.5	48.4	2.528
5.0	296.4	150.4	---	---	20.5	1348.8	168.7	---	2.541
6.3	346.7	159.7	---	2.549	21.2	1395.6	162.7	---	2.507
6.5	397.3	167.1	48.9	---	22.0	1447.9	184.9	47.0	2.538
7.2	448.0	172.9	---	---	22.6	1497.4	174.4	---	2.527
7.9	498.6	156.8	---	---	23.0	1547.2	180.7	---	---
8.6	547.9	166.0	45.3	---	23.6	1595.9	182.0	---	---
9.3	598.1	163.1	---	---	24.4	1645.8	185.0	48.4	---
10.0	648.8	147.8	---	---	25.1	1696.5	180.4	---	---
10.7	697.1	174.2	48.9	---	25.8	1749.2	158.8	---	---
11.4	746.4	162.7	---	---	26.5	1796.2	168.0	48.5	---
12.1	796.8	153.2	---	---	27.2	1847.3	187.6	---	---
12.9	848.6	177.4	47.0	---	27.9	1897.4	169.2	---	---
13.5	896.5	163.9	---	2.508	28.6	1945.4	162.9	46.3	---
14.2	947.7	174.5	---	2.491	29.3	1996.4	186.2	---	2.502
15.0	996.5	152.9	47.0	2.490	30.0	2046.8	155.7	---	2.521
16.3	1046.1	158.5	---	2.490	30.8	2098.1	160.2	50.2	---
17.0	1096.6	164.1	---	2.516	31.5	2146.0	148.7	---	2.511
17.6	1178.2	177.6	---	---					

Table A.7 Mechanical Testing Results of I90 Cylinders

Age (days)	Maturity (°C-days)	f_c (MPa)	E (GPa)	Density (g/cm^3)	Age (days)	Maturity (°C-days)	f_c (MPa)	E (GPa)	Density (g/cm^3)
1.2	32.4	119.7	---	2.504	11.3	943.5	170.6	---	2.526
1.3	33.3	122.9	42.5	2.499	11.8	992.7	164.0	48.3	---
1.4	47.1	144.1	---	2.503	12.4	1044.2	185.8	---	2.535
1.5	58.4	145.2	48.6	2.496	12.9	1093.7	175.3	---	2.529
1.5	59.0	146.3	---	2.487	13.5	1142.2	161.3	48.3	---
1.6	69.8	160.3	---	2.462	14.0	1192.1	163.2	---	2.489
1.7	80.6	145.4	---	2.487	14.6	1242.9	180.1	---	2.531
1.7	80.6	138.3	44.4	2.483	15.1	1291.9	198.2	49.3	---
2.1	93.6	154.6	46.4	---	15.7	1344.5	176.3	---	2.500
2.6	141.3	155.7	---	2.498	16.2	1393.9	133.0	---	2.491
3.2	193.0	155.0	---	2.529	16.8	1443.7	180.5	48.1	2.514
3.8	243.1	146.2	46.1	---	17.4	1494.8	187.9	---	2.522
4.3	291.9	166.2	---	2.507	18.0	1546.4	189.1	---	2.503
4.9	343.4	160.4	---	2.517	18.5	1593.1	193.3	48.7	---
5.4	391.4	131.4	47.4	2.523	19.0	1644.8	183.6	---	2.495
5.8	445.3	175.7	---	2.533	19.6	1694.5	198.8	---	2.500
6.3	494.1	178.6	---	2.518	20.3	1744.5	196.7	47.9	---
6.9	543.7	153.3	44.8	---	20.8	1793.5	140.0	---	---
7.4	591.6	166.8	---	2.495	21.4	1844.1	189.8	---	---
8.0	642.1	194.0	---	2.545	22.0	1894.3	209.8	48.1	---
8.5	691.8	173.9	48.1	---	22.4	1944.2	194.6	---	2.527
9.0	740.9	166.4	---	---	22.9	1993.6	192.4	---	2.500
9.7	796.5	201.2	---	2.510	23.4	2042.0	150.8	49.7	2.533
10.3	844.5	169.2	49.2	---	24.0	2092.3	172.1	---	2.489
10.8	896.2	153.8	---	2.510	24.5	2142.2	187.9	---	2.477